AN INVESTIGATION OF THE CRACK PROPAPAGATION MODEL CORPUS

by

Fazıl Önder Sönmez

B.S. in M.E., Boğaziçi University, 1988

Submitted to the Institute for Graduate Studies in

Science and Engineering in partial fulfilment of

the requirements for the degree of

Master of Science

in

Mechanical Engineering

Boğaziçi University
February, 1991

AN INVESTIGATION OF THE CRACK PROPAGATION MODEL CORPUS
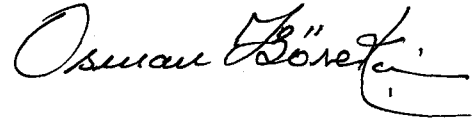
APPROVED BY :

Prof. Dr. Öktem Vardar
(Thesis Supervisor)

Prof. Dr. Akın Tezel

Y. Doç. Dr. Osman Börekçi

DATE OF APPROVAL : 21.2.1991

ACKNOWLEDGEMENT

I would like to express my deep appreciation to Professor Öktem Vardar for his helpful advice, encouragement and guidance throughout this study.

ABSTRACT

Models that predict fatigue crack growth are described, classified and compared with respect to applicability and limitations. Crack opening models were found to be more reliable and better adapted to include interaction effects that determine the extent of fatigue crack growth.

The CORPUS crack propagation model, the most sophisticated one among the crack opening models has been qualitatively and quantitatively analyzed.

A computer program of the model has been developed and run for a number of flight simulation spectra. The prediction results have been compared to the data given by de Koning, originator of the model, and Padmadinata, another investigator, and agreement has been observed.

A comparison between experiments and prediction results has been made, consistencies and discrepancies as to the trends of crack growth for variations of spectrum and test parameters are indicated.

Finally, several recommendations for possible improvement of CORPUS model are given.

ÖZET

Çatlak yorulmasını tahmin eden modeller tanımlandırılıp ve sınıflandırılıp, uygulanabilirlilik ve uygulama sınırları hususlarında karşılaştırıldı. Çatlak açılma modellerinin, daha güvenilir ve yorulma çatlaklarının büyümesini kontrol eden etkileşim etkenlerini içermeye daha elverişli olduğu görüldü.

Çatlak açılma modelleri arasında en karmaşık ve en ileri olan CORPUS çatlak ilerleme modeli nitel ve nicel olarak analiz edildi.

Modelin bir bilgisayar programı yapıldı ve uçuş benzetme spektrumunda çalıştırıldı. Modelin tasarlayıcısı de Koning ve ve diğer bir araştırmacı olan Padmadinata'nın sağladıkları veriler, tahmin sonuçları ile karşılaştırıldı ve birbirleri ile uyuştukları görüldü.

Deney ve tahmin sonuçları arasında karşılaştırma yapıldı. Spektrum ve test parametrelerinin değişimi ile olan çatlak büyüme eğilimleri bakımından uyum ve uyumsuzluklar belirtildi.

Son olarak, CORPUS modelinin geliştirilmesi için tavsiyeler verildi.

TABLE OF CONTENTS

LIST OF FIGURES

LIST OF TABLES

LIST OF SYMBOLS

a	half crack length
a_{OL}	crack length when overload is applied
a_p	overload induced plastic zone size plus crack length when the overload applied
Δa	crack growth increment
b	half specimen width
C	constant in the Paris relation for crack growth rate
CA	constant amplitude
C_p	scaling parameter used in Wheeler model
da/dN	cyclic crack growth rate
D	plastic zone size
D_{OL}	overload induced yield zone size
D_{an}	plane strain plastic zone size (CORPUS model)
D_{ss}	plane stress plastic zone size (CORPUS model)
eff	effective
eq	equivalent (ONERA model)
EF	sequence efficiency
f_1 , f_2	K_{op} / K_{max} (R) functions (ONERA model)
h	correction function accounting for yield stress effect (CORPUS model)
K	stress intensity factor
K_c	fracture toughness
K^*_{max}	the amount of stress intensity that would cause plastic zone to reach a_p
ΔK	range of stress intensity factor (K_{max} - K_{min})
ΔK_{eff}	range of effective stress intensity factor (K_{max} - K_{op})
KH	memorised stress intensity factor
l	fictitious half crack length in Newmans model
m	-exponent to shape scaling parameter C_p , (Wheeler model) -exponent used in Forman and Walker equations for stress ratio
n	exponent in the Paris relation

n	exponent in the Paris relation
$\dot{m}^n$	relaxation factor (CORPUS model)
$\dot{m}^n_{st}$	stationary value for relaxation factor (CORPUS model)
N	cycle
op	opening
OL	overload
R	stress ratio ($\sigma_{min} / \sigma_{max}$)
red	residual
SPZ	secondary plastic zone (CORPUS model)
t	thickness of specimen
TH	threshold
U	$\Delta\sigma_{eff} / \Delta\sigma = \Delta K_{eff} / \Delta K$
W	width of specimen
Y	correction factor accounting for finite width
α	load spectrum parameter (ONERA model)
β	ratio used for reducing effective overload stress intensity factor for underload cases
σ_a	stress amplitude
σ_{gr}	ground stress
σH	memorized stress
σ_{max}	maximum stress
σ_{min}	minimum stress
σ_{op}	opening stress
σ_{YS}	yield stress
Φ_R	proportionality factor for K_{red} (Multi parameter yield zone model)
Φ_A	proportionality factor for K_{red} used for acceleration adjustment(Multi parameter yield zone model)

I. INTRODUCTION

Mechanical components, vehicles, buildings are generally subjected to loads varying with time. Small, carefully manufactured mechanical components will not contain any flaw and majority of their life is consumed in nucleating a small crack. However large structures, especially welded ones, unavoidably contain cracks at the beginning of their service lives. These cracks are liable to grow and cause catastrophic failures. Therefore, cracks should be designed propagate at rates low enough to allow them to be detected and repaired before adjacent structures can no longer bear limit loads. In that respect, there is an obvious need for analytical models that predict growth rate of cracks in structures.

There are various types of prediction models with varying degrees of predictive capacity, yield zone models (discussed in chapter III), characteristic-K models (chapter, IV), strip yield models (chapter V), non-interaction models (chapter VII), crack opening models (chapter VIII). Among these, the crack growth prediction models based on crack opening seem to provide the most accurate and reliable results.

The aims of the present investigation are:

1. A general discussion and evaluation of crack growth prediction models.

2. A detailed analysis of CORPUS crack propagation model.

3. A computer program of the CORPUS model that has been verified by applying several flight simulation spectrums.

4. A discussion of the performance of the CORPUS model.

II. FATIGUE CRACK GROWTH

The fatigue life of engineering materials can be divided into three phases; initiation, propagation, and final failure. During the initiation stage, the process is highly susceptible to the influence of local factors such as dislocations, inclusions and grain boundaries and this stage constitutes most of fatigue life [1]. (Figure 2.1). But later, after some growth the influence of local material structure will decrease. Finally, bulk properties of the material will become important and the stress/strain distributions will be significantly affected by the crack itself. Stress intensity factor K then gains real meaning and significance. The final crack occurs when the macrocrack grows and the remaining parts can no longer support the load. In the present study interest lies with macrocrack propagation.
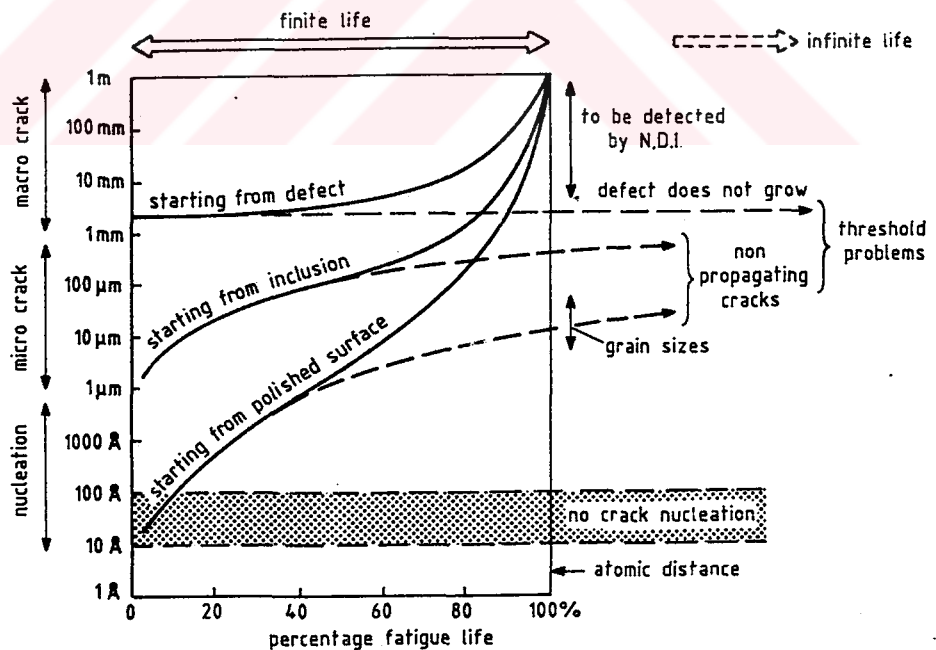
Figure 2.1: Different regimes of fatigue crack growth [1]

2.1   General Characteristics of Macrocrack Growth

A number of aspects of macrocrack growth should be summarised, as they are relevant to the assumptions made in the crack growth prediction models to be discussed later.

2.1.1   Striations

Fatigue surfaces have extensively been studied using electron microscopes. The prominent feature of fatigue fracture surfaces is that of distinct line markings, approximately parallel to one another and normal to the direction of crack growth. These are generally called striations; each striation corresponds to one load cycle, although not every load cycle necessarily results in a striation (Figure 2.2). This phenomenon has led to prediction techniques to calculate crack growth cycle-by-cycle.
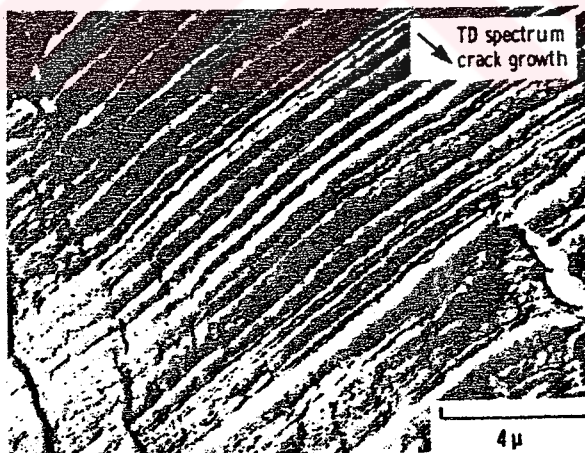
Figure 2.2: A typical   pattern of striations on a fatigue
fracture surface in a random spectrum, which
illustrates crack extension cycle-by-cycle [2].

2.1.2 The Similitude Approach and Stress Ratio Effects

The application of fracture mechanics to fatigue crack growth is based on the similitude concept employing the stress intensity factor K. The basis for the use of the stress intensity is that equal stress intensities result in equal mechanical crack tip environments. As a consequence, the crack extensions (da/dN) will also be the same. It should be noted that several attempts have been made to relate crack growth to other similitude criteria, such as crack tip strain [3] and crack opening displacements [4]. If we choose K as a similitude criteria, we may expect da/dN to be a function of K_{max} and K_{min}, ignoring wave shape and frequency effects.

$$\frac{da}{dN} = f(K_{max}, K_{min}) \qquad (2.1)$$

or, equivalently,

$$\frac{da}{dN} = f(\Delta K, R) \qquad (2.2)$$

where ΔK is the stress intensity range and R is the stress ratio.

$$\Delta K = K_{max} - K_{min} \qquad (2.3)$$

$$R = \frac{K_{min}}{K_{max}} \qquad (2.4)$$

Paris & Erdogan [5] derived a power relation, ignoring the R-effect, between crack growth (da/dN) and stress intensity range (ΔK).

$$\frac{da}{dN} = C\,\Delta K^n \qquad (2.5)$$

But, in general, three distinct types of behaviour occur in fatigue crack propagation. As shown in Figure 2.3 growth rate vs. ΔK curve is a sigmoidal shape. Region I is the low ΔK end of the curve where growth rate decreases rapidly with decreasing ΔK and approaches lower limit at ΔK_{TH} Region II is the midrange of crack growth rates where the power law dependence prevails. Region III is the high ΔK end of the curve where K_{max} approaches K_c. Figure 2.3 also shows that the stress ratio effect is particularly pronounced in regions I and III.
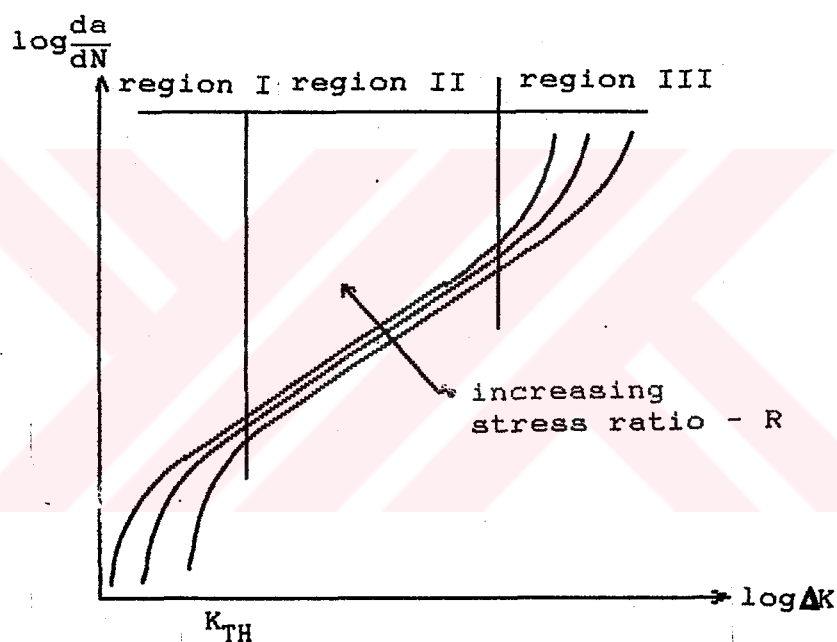
Figure 2.3: A typical crack growth curve and effect
of stress ratio on crack growth

2.1.3 Crack Closure

Crack closure under cyclic tension was discovered by Elber in 1970 [6]. He observed that crack faces can close on each other even under a tensile applied stress. This was attributable to plastic deformation left behind the advancing fatigue crack. He assumed that crack growth only occurs during

the time when the crack is open. Thus, an effective stress intensity factor range is defined through

$$\Delta K_{eff} = K_{max} - K_{op} \qquad (2.6)$$

where K_{op} corresponds to the point at which the crack is fully open. The Paris law (eq.2.5) then becomes

$$\frac{da}{dN} = C (\Delta K_{eff})^n \qquad (2.7)$$

Under variable amplitude loading, the crack closure concept may account for both crack retardation and acceleration effects as shown in Figure 2.4.
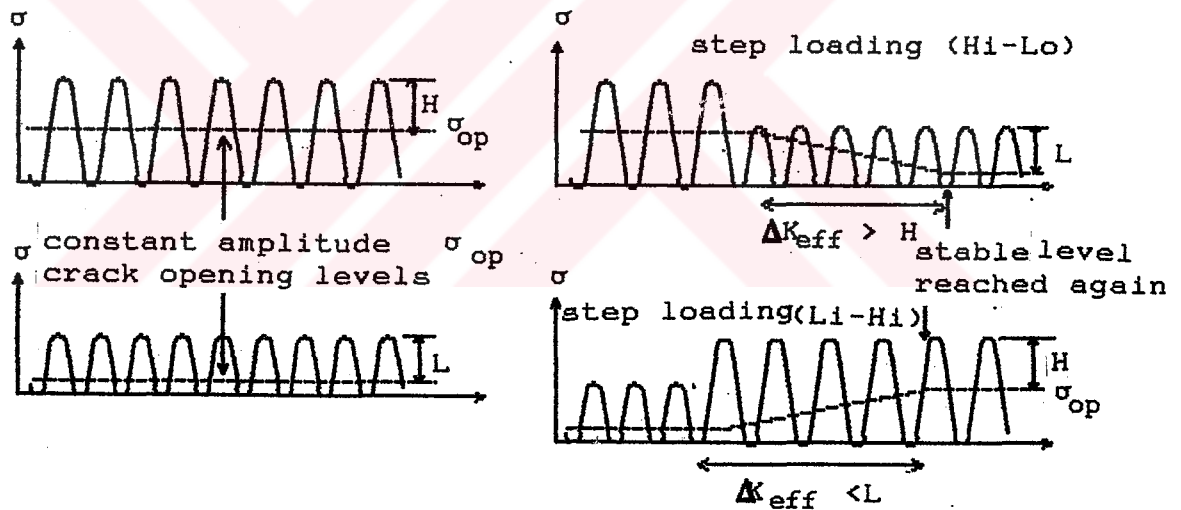
Figure 2.4: Explanation of acceleration and retardation through crack opening concept [1]

2.1.4 Crack Tip Blunting

Crack tip blunting can occur if a high overload is applied. Crack tip blunting causes crack growth acceleration following an overload due to reduction of crack closure. In

other words, the crack tip blunting does not lead to acceleration during the overload cycle itself, but results in an initial acceleration after the load (Figure 2.5).
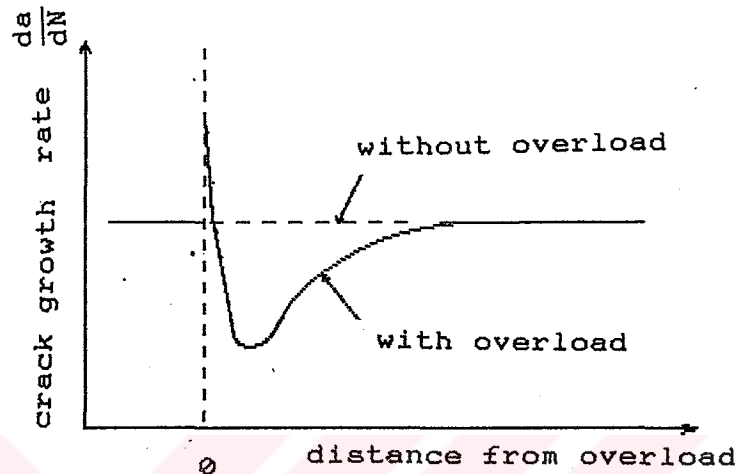
Figure 2.5: Initial acceleration following an overload cycle [3]

2.1.5 Thickness Effect

Thickness has an important effect on the plastic zone size and crack tip state of stress, namely plane stress / plane strain or in between. Plastic zone size is approximately three times larger under plane stress conditions. For a thick specimen, the state of stress is depicted schematically in Figure 2.6 [8]. Due to the absence of constraints on free surfaces, the plane stress condition dominates. Larger plastic zones imply more deformation left in the wake of the growing crack and hence more crack closure. A faster crack growth under plane strain conditions implies that a thick specimen will show less closure than a thin specimen due to different degrees of plasticity (Figure 2.7) [9]. In his model, De Koning [10] assumes plane strain conditions if the ratio of plastic zone size to thickness is less than 0.35 and plane stress condition, if the ratio exceeds 0.5.
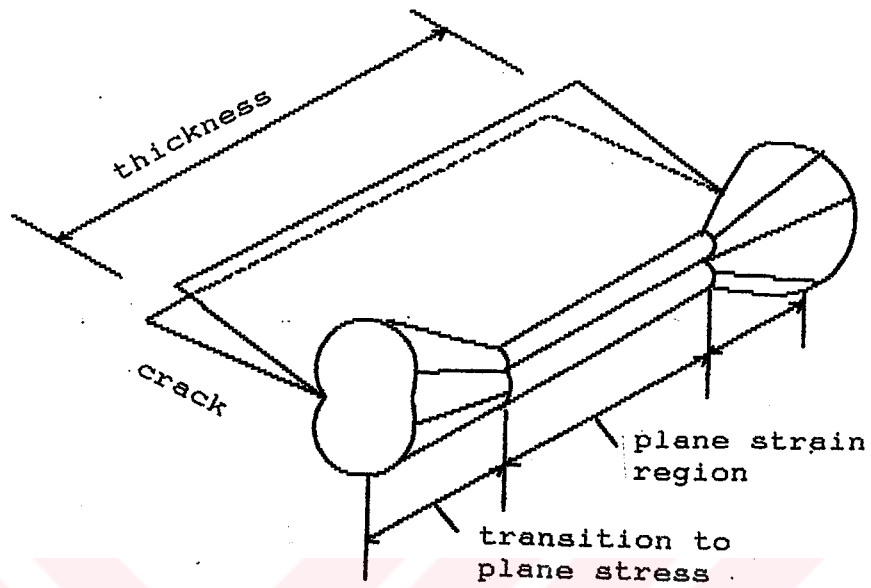
Figure 2.6: Schematic representation of the plastic zone
variation along the thickness[8]
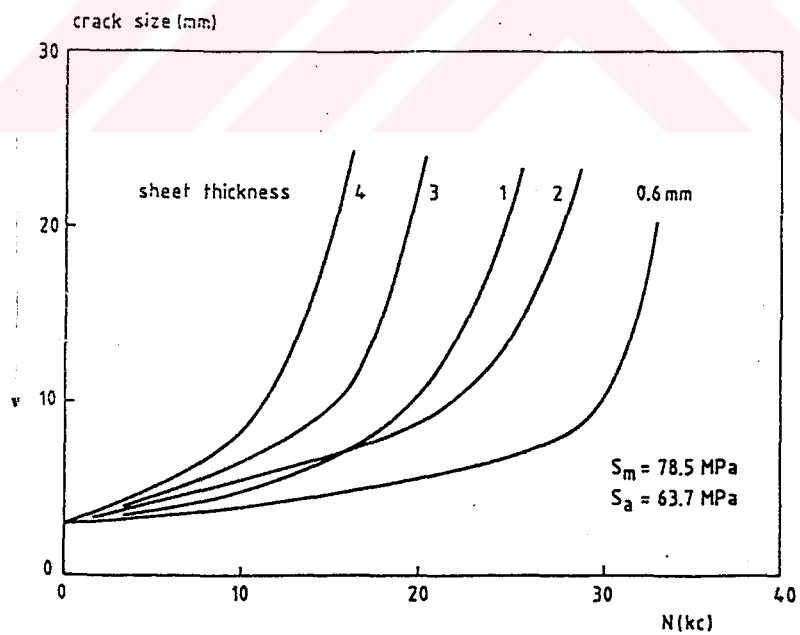
Figure 2.7: Influence of sheet thickness on crack growth[9]

2.1.6 Environmental Effects

Aggressive environments tend to increase growth rates for those materials which are susceptible [11]. Crack growth does not take place at values of ▲K significantly less than that corresponding to a growth rate of one lattice spacing per cycle. However, this does not necessarily apply in the presence of a corrosive environment. In other words, crack growth in a corrosive medium may take place at very low values of ▲K [12].

2.1.7 Wave Shape and Frequency Effects

Cyclic wave form and frequency have no observable effect on fatigue crack growth [13]. However tests on 2024 Aluminum alloy sheet specimens shows that growth rate at higher frequencies tend to be slightly lower than the growth rate at lower frequencies [14].

2.1.8 Temperature Effect

Elevated temperatures accelerate fatigue crack growth. Moderately low temperatures tend to have a retardation effect on crack growth [3].

2.1.9 Crack Front Geometry

In general, it is assumed in fracture mechanics analyses that a fatigue crack is a flat mode I crack; if it is a through crack with a straight-single line crack front. Two phenomena can disturb this simplified picture: crack branching and shear lips.

Usually fatigue microcracks grow perpendicular to the main principle stress (mode I). However, when the crack driving force is low (i.e. when it is difficult to extend the crack) deviations from that direction may occur on a microscopic

level. This can lead to a kinked crack path and sometimes to crack branching (Figure 2.8). Such conditions can occur after an overload. In such cases, the magnitude of stress intensity factor decreases. A reduction of the crack growth rate is then due to a lower crack driving force which will contribute to crack growth retardation [15].

a) Kinked crack

b) Forked Crack

c) Zig-Zag crack

d) Twisted crack
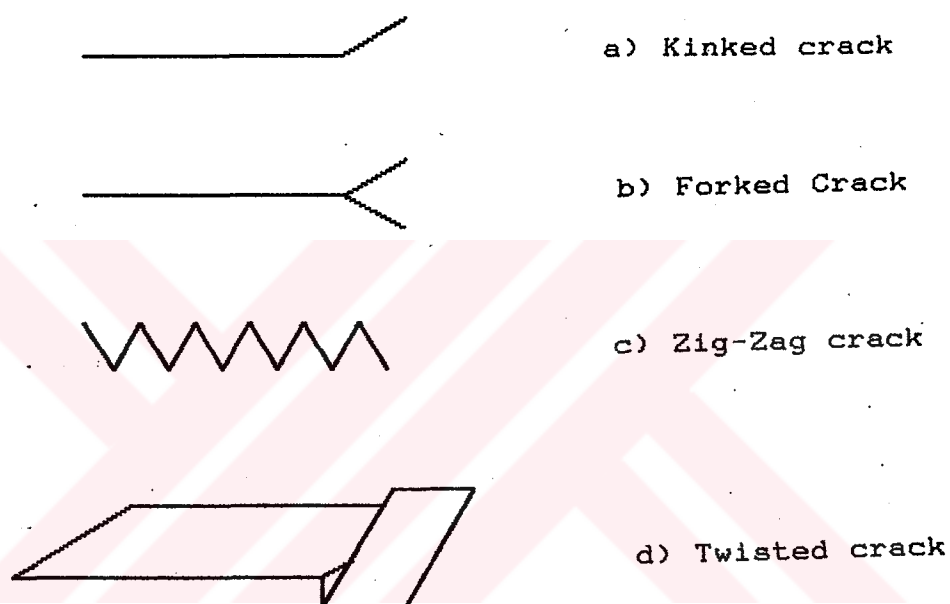
Figure 2.8: Types of crack front abnormalities[15]

Another complication of the crack front geometry is the occurrence of shear lips (Figure 2.9). It should be expected that crack closure will be more predominant at the shear lips than for the core material. This is a consequence of the larger plastic zones (plane stress) at the material surface. Removal of surface material of a fatigue cracked specimen reduces σ_{op} [16]. Another consequence of shear lips is that the crack front is no longer a straight line, mixed mode cracking (I and III) is seen to occur. This implies that the K factor for mode I cannot give a correct indication of the crack driving force.

Particularly for variable amplitude loading incompatible crack fronts can easily occur.
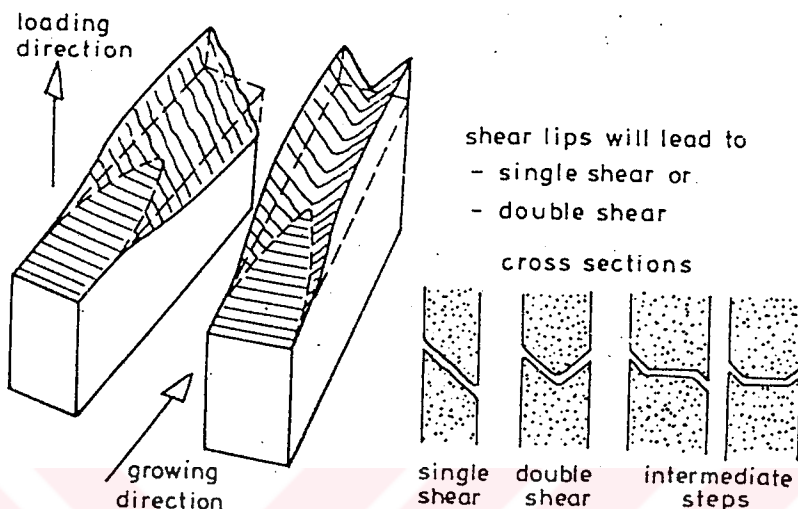
Figure 2.9: Shear Lips [1]

2.1.10 Stress Pattern at the Crack Tip

The Stress pattern at the crack tip is important in understanding fatigue crack growth. Residual stresses acting at the crack tip are considered as another possibility leading to retarded growth. Non uniform stress distributions at the crack tip will induce residual compressive stresses upon unloading from a peak load as shown in Figure 2.10.

2.1.11 Interaction Effects

Various simple variable amplitude load sequences have been adopted in the literature, such as single overload, multiple overloads, underloads. Trends of load interaction effects observed in such test are summarised below.
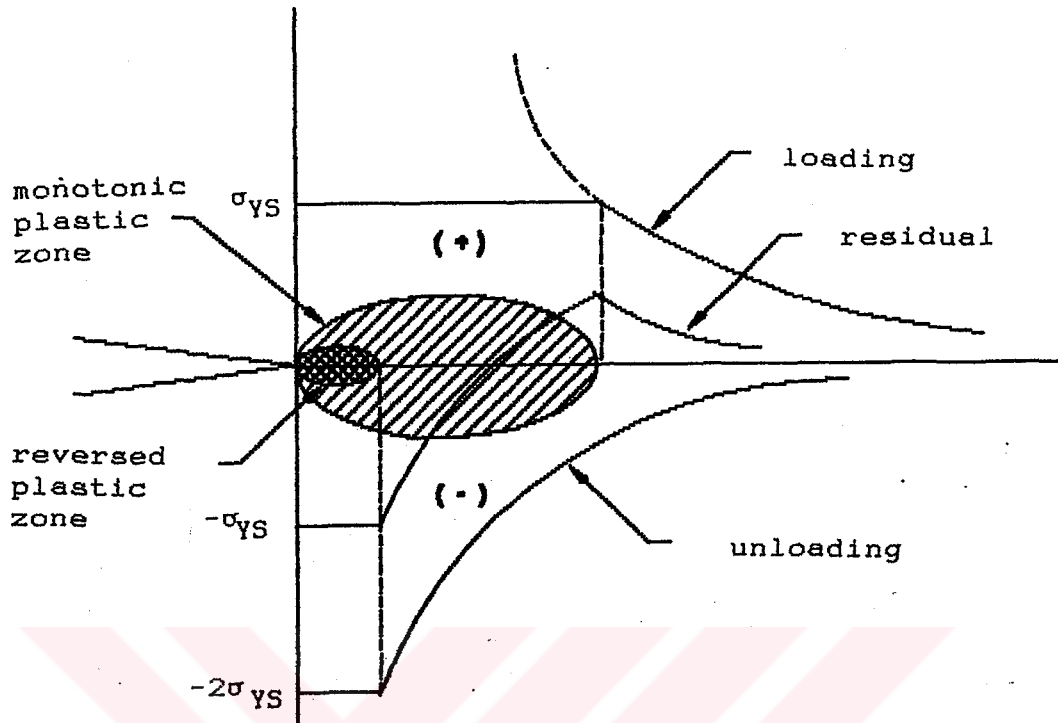
Figure 2.10: Stress pattern at the tip upon a cycle of
loading and unloading[8]

2.1.11.1 Single Overload

A. single overload induces significant crack growth
retardation (Figure 2.11) [17,18]. There is an initial
acceleration observed in some cases right after the overload.
Retardation is not immediate even if acceleration does not take
place. The original rate continues over a small distance and
the retardation is called "delayed retardation". If the
overload is strong enough, crack arrest or abnormally low
growth rate is observed.

2.1.11.2 Intermittent Overloads

When tensile overloads are applied periodically the
resulting retardation depends on the interaction between these
overloads [19]. If these overloads are far away from each other
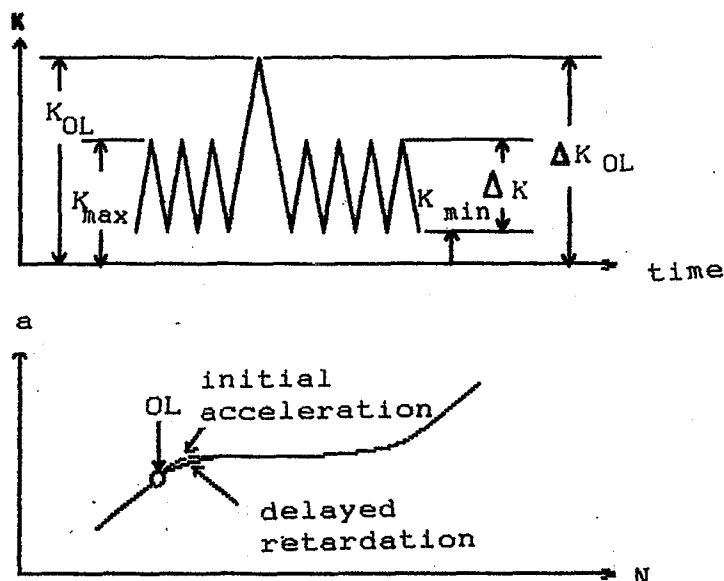
Figure 2.11: A Typical Single Overload case and The
Resulting Retarded Growth [17]

they act as isolated events. Maximum retardation is claimed to
occur when the crack extension between the overloads is about
one fifth of the plastic zone size of the first overload [20].

2.1.11.3 Multiple Overloads

Multiple overloads increase the amount of retardation.
(Figure 2.12) [11]. Overload interactions result in higher
crack opening levels for the overloads. The crack opening level
increases with increasing number of overload cycles until a
saturation level has been reached [10].

2.1.11.4 Underload Effects

Underloads tend to negate retardation effects of
overloads. If an underload precedes a positive overload the
reduction of the delay is small, but if it immediately follows
a positive overload, crack growth delay is significantly
reduced [21]. Moreover, a crack arrested at the threshold

σ

σ^1

σ^2

A

σ

σ^1

σ^2

B

$\frac{da}{dN}$ yield zone Δa

A

B
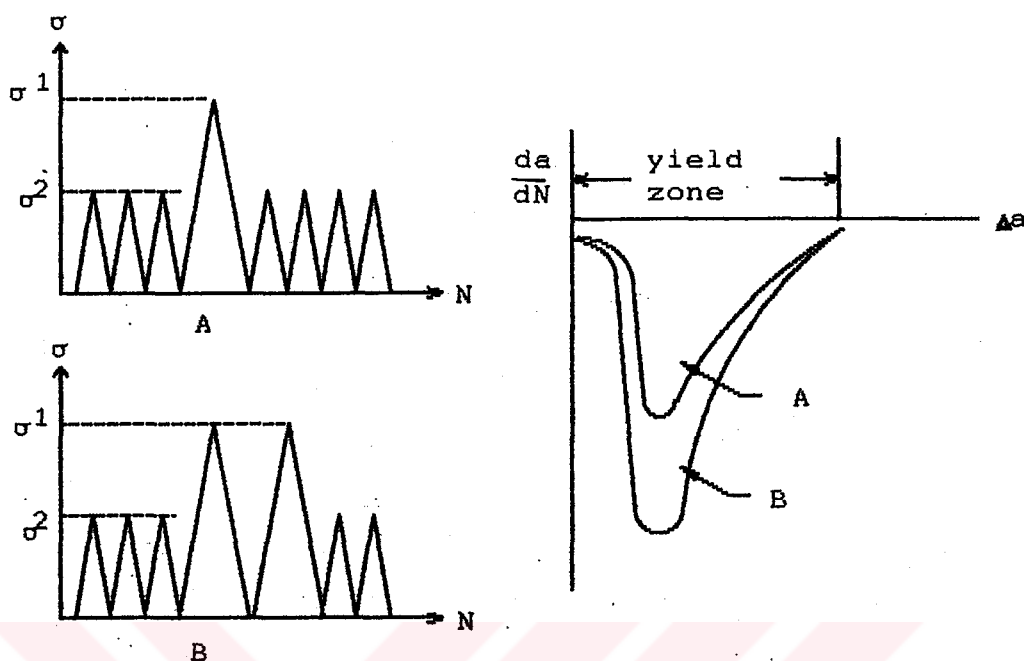
Figure 2.12: Multiple overload retardation [11]

(ΔK_{TH})

can be propagated through the application of periodic compression cycles.

2.2 Flight Simulation Sequences

Flight-simulation testing is a generally accepted fatigue testing procedure in aeronautics. Flight-simulation load histories should reflect real load histories, which can occur during its life time. A flight simulation load history thus must consist of a flight-by-flight sequence. Usually, the cyclic loads in one flight are a superposition of deterministic and stochastic loads. The load history applied in the test is a time-condensed version of the real time history, obtained by (1) omitting the parts during which the load does not vary, (2) omitting small cycles which are supposed to be insignificant for fatigue damage, and (3) by increasing the load frequency. The load history in a flight simulation test must be representative for a certain aircraft structure and assumed

utilization of the aircraft. Some standardized flight-simulation histories have been developed for general purposes (TWIST, FALSTAFF) and for specific aircrafts (F27, CN-235). Two flight-simulation load sequences (TWIST, F-27) are discussed below. Computer programs for these load sequences have been prepared for the verification of the computer program developed for the CORPUS crack propagation model.

2.2.1 TWIST

The TWIST standard represents the loading environment of lower wing skins of transport aircraft due to gust loading [22]. In one block, 4000 flights of ten different types (A to J in Table 1.1) occur in random sequence. The severity of the flights vary from light (type J, nice weather) to highly severe (type A, severe storm). The load spectrum of each flight can be obtained from Table 1.1. The continuous spectrum is approximated by a stepped function (10 amplitudes) for practical reasons. The amplitudes (σ_a) are related to the mean stress of the flights (σ_{mf}). The ground stress (σ_{gr}), i.e. the minimum stress of the ground-air-ground cycle (GAG) was standardized at $\sigma_{gr}=-0.5\sigma_{mf}$. The selection of the amplitude sequence is again randomly selected. Since experiments with TWIST were rather time consuming due to large average number cycles per flight, a shortened version, called miniTWIST [22], was generated. miniTWIST was derived from TWIST by omitting small amplitude cycles from the load spectrum as shown in Table 1.1. Figure 2.13 displays the difference between the two spectra in an exemple flight.

2.2.2 F-27

The F-27 flight simulation load history was generated by using exactly similar procedures adopted for TWIST and miniTWIST. The load spectrum is shown in Table 1.2. A sample of

the flight profile is given in Figure 2.14. In one block 2500
flight occurs (A to I) in a random sequence. The load history
was primarily generated by comparative studies, i.e. to study
the effects of σ_{mf}, of more or less severe σ_{gr}

TWIST flight 1 (H, 260 cycles)

miniTWIST flight 1 (H, 40 cycles)
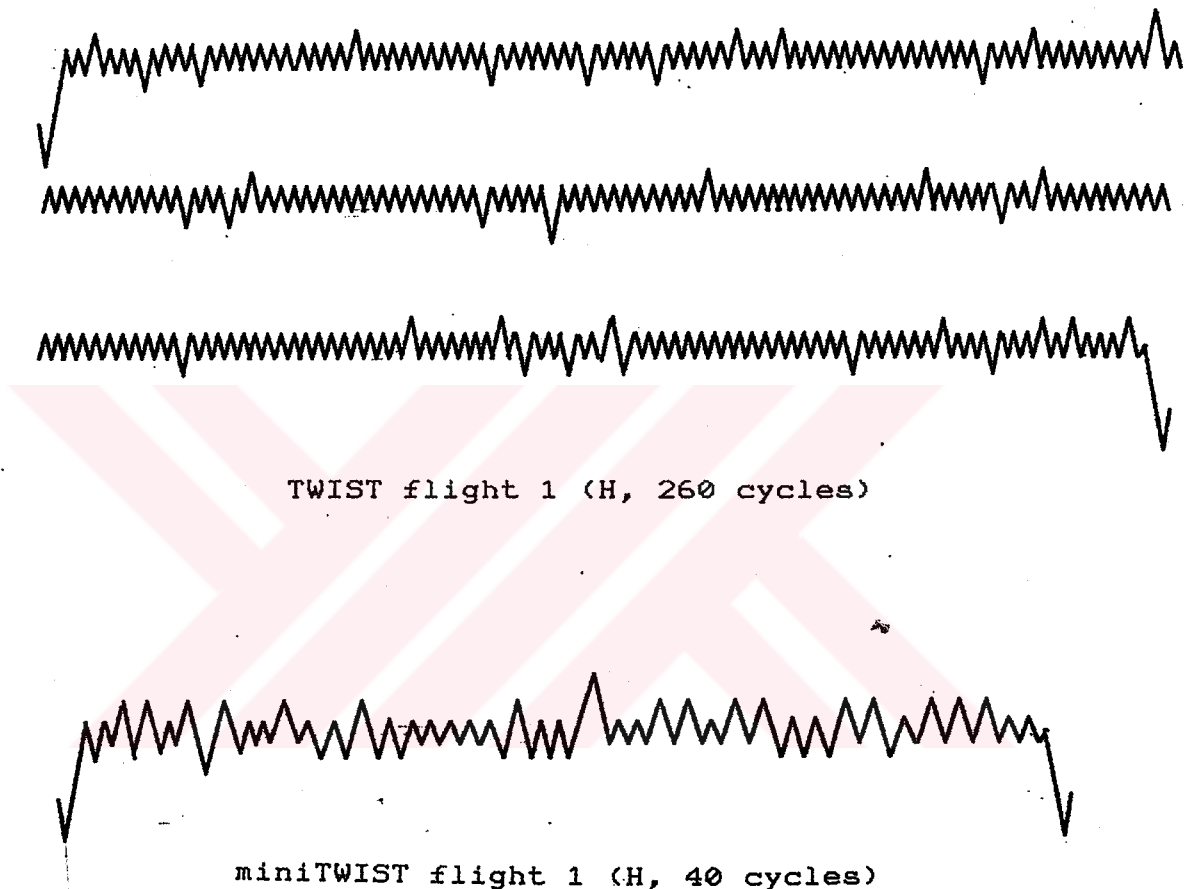
Figure 2.13: Generation of miniTwist by reduction of low
amplitude cycles.

2.2.3 F-4

The F-4 load sequence is an formerly used, simple one
amplitude load in flight, (see Figure 2.15). It is now
considered to be an unrealistic flight-simulation, which
probably gives rather conservative results.
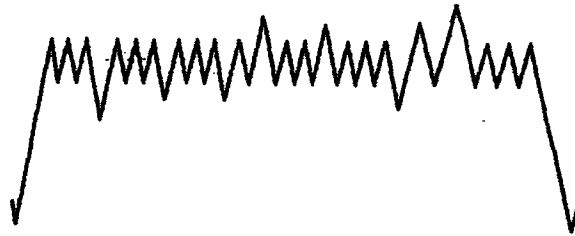
F-27 flight 6 (G, 18 cycles)

Figure 2.14: A sample of F-27 flight Profile
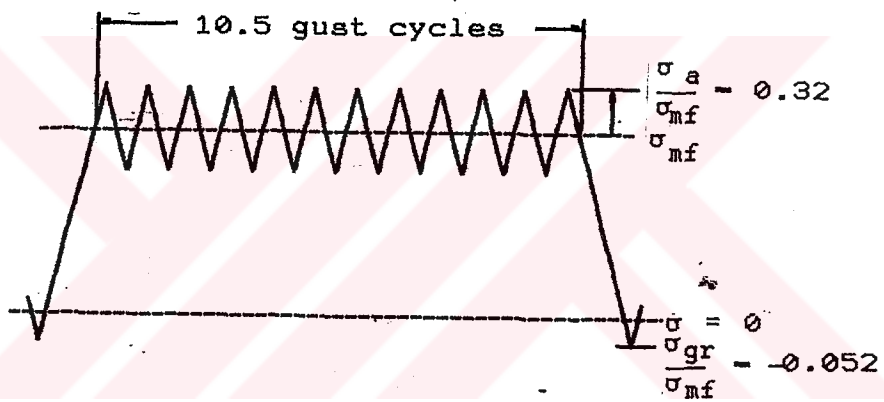
Figure 2.15: The F-4 load sequence. Gust cycles with
constant amplitude. All flights are equal. [7]

flight type	number of flights in one block	level and magnitude (σ_a/σ_{mf}) of magnitudes										total number of cycles per flight
		I 1.60	II 1.50	III 1.30	IV 1.15	V 0.995	VI 0.84	VII 0.685	VIII 0.53	IX 0.375	X 0.222	
		number of cycles per flight										
A	1	1	1	1	4	8	18	64	112	391 (391)	900 (0)	1500 (600)
B	1		1	1	2	5	11	39	76	366 (385)	899 (0)	1400 (520)
C	3			1	1	2	7	22	61	277 (286)	879 (0)	1250 (280)
D	9				1	1	2	14	44	208 (208)	680 (0)	950 (270)
E	24					1	1	6	24	165 (168)	603 (0)	800 (200)
F	60						1	3	19	115 (107)	512 (0)	650 (130)
G	181							1	7	70 (72)	412 (0)	490 (80)
H	420								1	16 (16)	233 (0)	250 (40)
I	1090									1 (1)	69 (23)	70 (5)
J	2211										25 (2)	25 (2)
cycle per block of 4000 flights		1	2	5	18	52	152	800	4100	34800 (34800)	358665 (18442)	
cumulative of cycles		1	3	8	26	78	230	1030	5200	40000	398665 (58442)	

Average Number of Cycles per Flight = 100 (15) $\sigma_{gr} / \sigma_{mf} = -0.5$

Table 1.1: TWIST (miniTWIST) flight simulation spectrum.

flight type	number of flights in one block	level and magnitude (σ_a/σ_{mf}) of magnitudes										total number of cycles per flight
		I 1.25	II 1.15	III 1.05	IV 0.95	V 0.85	VI 0.75	VII 0.65	VIII 0.55	IX 0.425	X 0.30	
		number of cycles per flight										
A	1	1	0	1	0	2	0	3	5	7	28	47
B	1		1	0	1	0	2	2	4	7	27	44
C	2			1	0	1	1	2	3	7	25	40
D	4				1	0	1	2	2	6	24	36
E	11					1	1	0	3	4	23	32
F	27						1	1	2	4	20	28
G	70							1	1	2	18	22
H	184								1	1	14	16
I	2200									1	9	10
cycle per block of 2500 flights		1	1	3	5	15	46	114	364	2728	24630	
cumulative of cycles		1	2	5	10	25	71	185	549	3277	27907	

Average Number of Cycles per Flight = 11

(case: normal gust, normal σ_{gr})

$\sigma_{gr} / \sigma_{mf} = -0.234$ for 2024-T3 $\sigma_{gr} / \sigma_{mf} = -0.254$ for 7075-T6

Table 1.2: F-27 Flight Simulation Load Spectrum

III. YIELD ZONE MODELS

These models [23,24,25,26,27,28] assume retardation to persist as long as the crack tip plastic zones for subsequent load cycles are within the peak load plastic zone. They explain retardation as a function of overload and current plastic zone.

3.1. WHEELER MODEL [23]

The Wheeler model predicts retardation by reducing the crack growth rate within the plastic zone created by an overload and uses a factor to suppress crack growth calculations following an overload. The crack growyh increment is given by

$$a^n - a_0 + \sum_{i-1}^n C_p^i \ f(\Delta K^i) \tag{3.1}$$

where $f(\Delta K^i)$ is the linear constant amplitude growth function and C_p is defined as,

$$C_p^i - \left(\frac{D^i}{a_{OL} + D_{OL} - a^i} \right)^m \quad if \ a^i + D^i \preceq a_{OL} + D_{OL} \tag{3.2}$$

$$C_p^i - 1 \quad if \ a^i + D^i \succ a_{OL} + D_{OL} \tag{3.3}$$

$$D^i - \frac{1}{\alpha} \left(\frac{K^i}{\sigma_{YS}} \right)^2 \qquad \alpha - \left(\begin{array}{l} \dfrac{1}{4\pi} \ for \ plane \ strain \\[2mm] \dfrac{1}{2\pi} \ for \ plane \ stress \end{array} \right) \tag{3.4}$$

where D_{OL} is the overload induced yield zone, D^i is the extent of the current yield zone (Figure 3.1) and m serves as a shaping factor. C_p is bounded between zero and one. It takes its minimum value after the application of the overload and gradually increases until the current yield zone moves out of the previously overload induced yield zone.

The exponent m provides the flexibility to shape the scaling parameter, C_p, to correlate with test data and must be established experimentally. m is constant for any particular case but varies depending on the type of material, specific loading conditions and possibly other factors. Forcing the shaping exponent to be a constant may provide a good correlation but a loss of generality is incurred in doing so. This causes Wheeler retardation model to be more a data fitting technique rather than a predictive model.
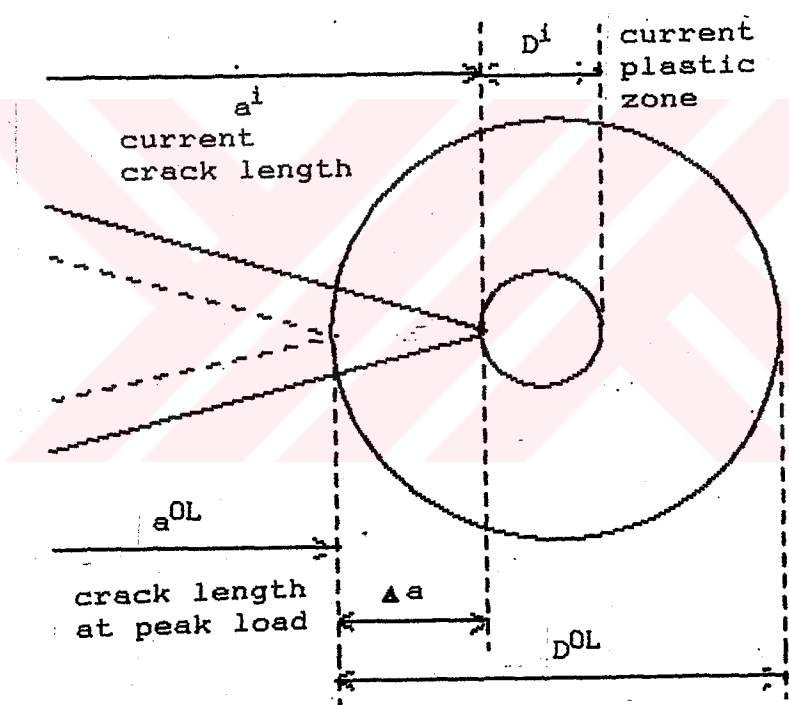
Figure 3.1: Crack Tip Yield Zones

3.2. WILLENBORG MODEL

· The Willenborg model uses CA crack growth rate data to model load interaction without relying on any other empirically derived parameters. The model assumes that retarded growth is related to residual stresses created by a previous overload. An empirically found residual stress is subtracted from both the maximum and minimum stresses. Retardation is proportional to the amount of this reduction. The length of the retarded growth is the zone of plasticity caused by the previous overload.
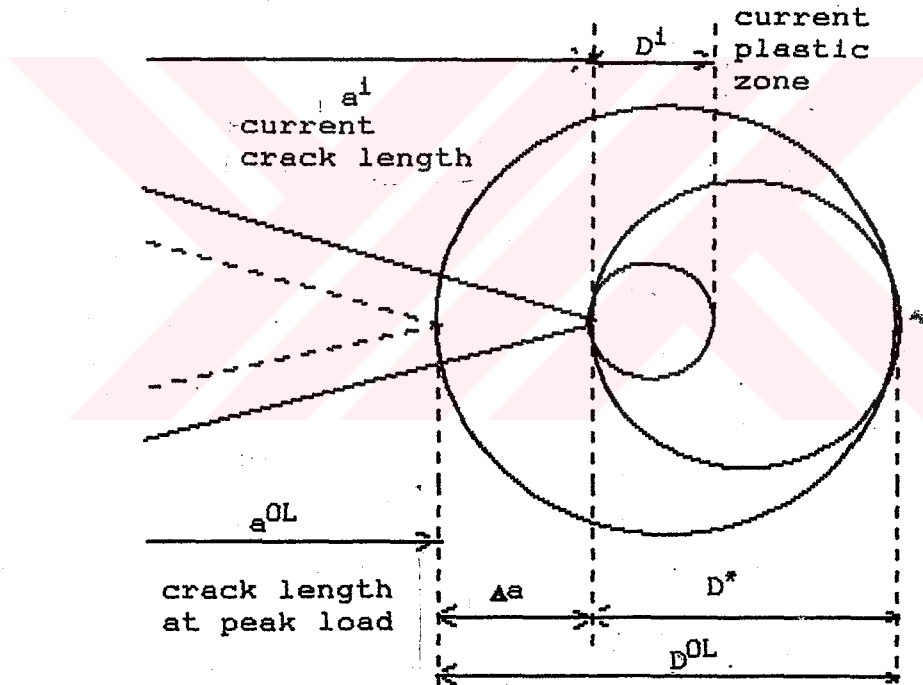
Figure 3.2: Yield zones after the application of overloads

The extent of the yield zone is given as,

$$D^i = \alpha \left(\frac{K^i}{\sigma_{YS}}\right)^2 \qquad \alpha = \left(\begin{array}{l} \dfrac{1}{3\pi} \quad \textit{for plane strain} \\ \dfrac{1}{\pi} \quad \textit{for plane stress} \end{array}\right) \quad (3.5)$$

The overload induces a plastic zone D_{OL} which extends to

$$a_p = D_{OL} + a_{OL} = \alpha \left(\frac{K_{max}^{OL}}{\sigma_{YS}} \right)^2 + a_{OL} \qquad (3.6)$$

The model assumes that as long as the current plastic zone is inside the peak load plastic zone there is retardation. As shown in Figure 3.2 D^* is the plastic zone that would be necessary in order to have no retardation. There is some stress intensty factor, K_{max}^*, which would cause a plastic zone D^* necessary for the plastic zone to reach a_p (Figure 3.3)

$$a^i + D^* = a_{OL} + D_{OL} \qquad (3.7)$$

$$D^* = a_{OL} - a^i + D_{OL} \qquad (3.8)$$

$$\alpha \left(\frac{K_{max}^*}{\sigma_{YS}} \right)^2 = a_{OL} - a^i + \alpha \left(\frac{K_{max}^{OL}}{\sigma_{YS}} \right)^2 \qquad (3.9)$$

Willenborg made the rather odd assumption that K_{max}^i will be reduced by the amount given by

$$K_{red}^i = K_{max}^* - K_{max}^i \qquad (3.10)$$

This means that both K_{max}^i and K_{min}^i are reduced by an amount K_{red}. Hence effective stress intensity is given by,

$$K_{maxeff}^i = K_{max}^i - K_{red}^i = 2K_{max}^i - K_{max}^* \qquad (3.11)$$
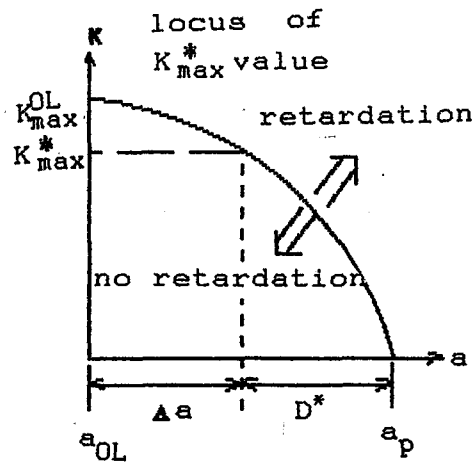
Figure 3.3: Stress intensity (K^*_{max}) that would cause plastic zone to reach a_p

$$K^i_{mineff} = K^i_{min} - K^i_{red} = K^i_{min} + K^i_{max} - K^*_{max} \qquad (3.12)$$

$$\Delta K^i_{eff} = K^i_{maxeff} - K^i_{mineff} \qquad (3.13)$$

If K_{mineff} or both K_{mineff} and K_{maxeff} turn out to be negative they are set to zero.

The cycle ratio, R_{eff}, becomes

$$R_{eff} = \frac{K^i_{min} - K_{red}}{K^i_{max} - K_{red}} \qquad (3.14)$$

After the calculation of ΔK_{eff} and R_{eff}, da/dN can be computed from the Forman equation.

$$\frac{da}{dN} = \frac{C \Delta K^n_{eff}}{(1 - R_{eff}) K_c - \Delta K_{eff}} \qquad (3.15)$$

Three distinct modes of retardation are possible for the Willenborg Model.

1) Both K^i_{max} and K^i_{min} are reduced by the same amount K_{red}, with positive outcome, leading to $\Delta K_{eff} = \Delta K$. But, R_{eff} being reduced slight retardation occurs.

2) K_{mineff} reduces to negative values so that $\Delta K_{eff} < \Delta K$. ΔK_{eff} is reduced and R_{eff} becomes zero.

3) Both K_{maxeff} and K_{mineff} reduce to negative values so that $\Delta K_{eff} = R_{eff} = 0$. In this case crack arrest occurs. The model predicts crack arrest at,

$$\frac{K^{OL}_{max}}{K_{max}} > 2 \qquad (3.16)$$

The Willenborg model does not account for the effects of multiple overloads and negative overload. His assumption that K^i_{max} is reduced by an amount $K_{red} = K^*_{max} - K^i_{max}$ is physically incorrect. Another shortcoming stems from the fact that the model treats each overload as a single discrete event. Hence, any cumulative effect is not accounted for. Acceleration effects are also not included.

3.3 MULTI-PARAMETER YIELD ZONE MODEL [26]

The present model attempts to account for <u>crack growth retardation</u> caused by previous overloads, <u>acceleration</u> due to current overloads and <u>underloads</u> resulting in a reduction of the retardation effects of the current overload.

The model uses a modified Forman crack growth equation.

for $\Delta K > \Delta K_{TH}$

$$\frac{da}{dN} = \frac{C\,\Delta K^n}{(1-R_{eff})^m\,K_c - \Delta K} \quad if \begin{pmatrix} 0 \le R_{eff} < R^+_{cut} & R_{eff} = R_{eff} \\ R_{eff} \ge R^+_{cut} & R_{eff} = R^+_{cut} \end{pmatrix} \quad (3.17)$$

for $\Delta K < \Delta K_{TH}$

$$\frac{da}{dN} = 0 \qquad (3.18)$$

where

$$m = 1 \quad at \ R \ge 0 \qquad (3.19)$$

$$m = 2 \quad at \ R < 0 \qquad (3.20)$$

ΔK_{TH} is the threshold stress intensity range and is a function of the effective stress ratio R_{eff} ,

$$\Delta K_{TH} = (1-R_{eff})\,\Delta K_{TH_0} \qquad (3.21)$$

In the equation above ΔK_{TH0} is the threshold value for R=0 case.

Eq. 3.17 uses the full stress intensity range (ΔK), that is the stress range includes the compressive portion. Load interaction effects are accounted for by adjusting R_{eff} during each cycle. Most of the procedures used in this model are concerned with finding proper values of R_{eff} to account for retardation, acceleration and underload effects.

R^+_{cut} is the cut-off value of the stress ratio that

limits the value of R_{eff} and is a function of the constraint at the crack tip due to the different stress states, that is plane stress/ plane strain or in between.

$$R_{cut}^+ = [\frac{D}{t} * 0.2] + 0.6 \qquad (3.22)$$

where

$$D = \alpha(\frac{K_{max}}{\sigma_{ys}})^2 \quad ; \quad \alpha = \left(\begin{array}{l} \frac{1}{3\pi} \quad \textit{for plane strain} \\ \frac{1}{\pi} \quad \textit{for plane stress} \end{array} \right) \qquad (3.23)$$

where D is the plastic zone diameter for the applied K_{max}.

In the model, load interaction effects are calculated utilizing a residual stress intensity (K_R) concept that is a modified version of the residual stress (K_{red}) used by Willenborg.

R_{eff} is given as

$$R_{eff} = \frac{K_{min} - K_R}{K_{max} - K_R} = \frac{K_{min_{eff}}}{K_{max_{eff}}} \qquad (3.24)$$

K_R will be negative or positive depending on whether the load interaction produces retardation or acceleration.

3.3.1 Retardation

In the model, the Willenborg residual stress intensity factor K_{red} is used.

$$K_{red}^i = K_{max}^* - K_{max}^i \qquad (3.25)$$

K^*_{max} is the stress intensity value which would cause a plastic zone D^* (Figure 3.4) that would be necessary for the plastic zone to reach a_p.
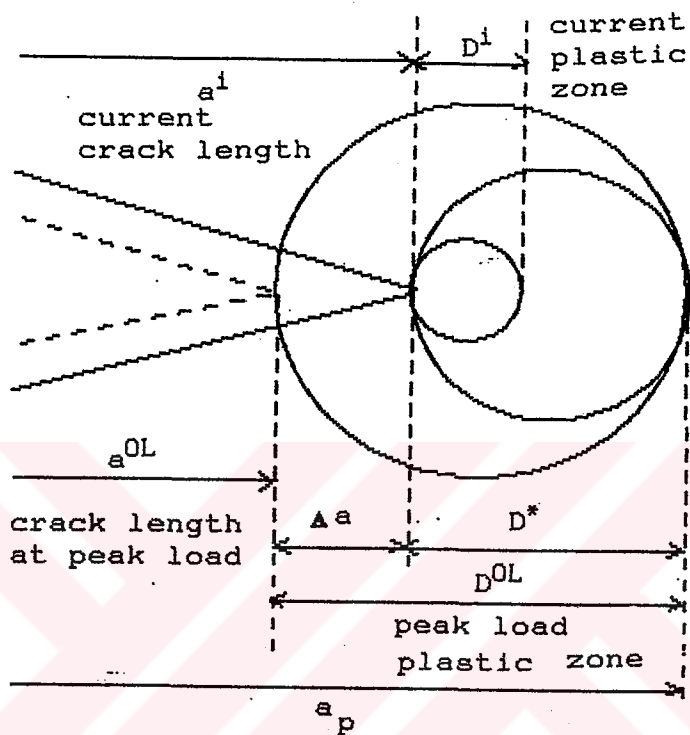
Figure 3.4: Plastic zones at the crack tip

$$D^* = a_{OL} - a^1 + D_{OL} \qquad (3.26)$$

$$D^* = -\Delta a + D_{OL} \qquad (3.27)$$

$$\alpha \left(\frac{K^*_{max}}{\sigma_{YS}} \right)^2 = (D_{OL} - \Delta a) \frac{D_{OL}}{D_{OL}} \qquad (3.28)$$

$$\alpha \left(\frac{K_{max}^{*}}{\sigma_{YS}}\right)^2 = \frac{(D_{OL} - \Delta a)}{D_{OL}} \alpha \left(\frac{K_{max}^{OL}}{\sigma_{YS}}\right)^2 \qquad (3.29)$$

$$K_{max}^{*} = K_{max}^{OL} \left(1 - \frac{\Delta a}{D_{OL}}\right)^{\frac{1}{2}} \qquad (3.30)$$

then

$$K_{red}^{i} = K_{max}^{OL} \left(1 - \frac{\Delta a}{D_{OL}}\right)^{\frac{1}{2}} - K_{max}^{i} \qquad (3.31)$$

Retardation effects extend over approximately one plastic zone diameter. Retardation occurs when K_{red} is positive. Figure 3.5 depicts a typical load sequence. The dashed line represents the decay in K^{*}_{max}.
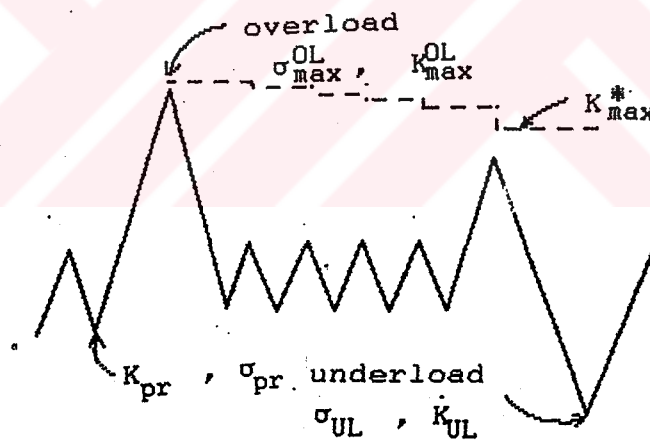
Figure 3.5: Sample spetrum sequence [26]

At this stage, the Willenborg residual stress intensity (K_{red}) is modified by a proportionality factor ϕ_R that adjusts the amount of retardation according to several material and load history parameters.

$$K_I = \phi_R K_{red} \qquad (3.32)$$

$$\phi_R = \frac{1 - \left(\dfrac{K_{TH_0}}{K_{max}}\right)}{(\delta - 1) * (1 - R_L)} \qquad (3.33)$$

where δ = S/A, A is the ratio of K^{OL}_{max} to K_{max} above which no crack growth is produced (shut-off ratio) and $R_L = \sigma_{UL} / \sigma^{OL}_{max}$ (ratio of current underload stress to current overload stress) as shown in Figure 3.5.

The $[1 - (K_{TH_0}/K_{max})]$ factor accounts for the threshold level of crack growth. The $(\delta - 1)$ factor adjust the retardation between the shut-off overload ratio S and the no-retardation ratio A as shown in Figure 3.6. The $(1 - R_L)$ expression adjusts the amount of retardation according to the cyclic range of the spectrum.
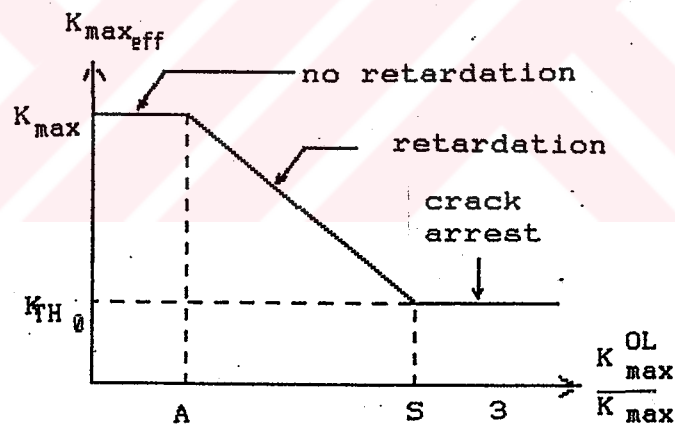
Figure 3.6: Schematic of retardation in the model [26]

Parameters A and S are considered to be material dependent parameters and are obtained from single overload tests.

The model accounts for multiple overload effects by lowering the value of S in the case of multiple overloads using an equation in which S is inversely proportional to the number of overloads applied in succession. This equation is also

material dependent.

3.3.2 Acceleration

The crack growth during an overload cycle is larger than one might expect from constant amplitude data. This phenomenon is referred to as crack growth acceleration. The acceleration is attributed in the model to the crack and the resulting crack tip plastic zone growing into an area with less residual stress intensity than that of an equivalent constant amplitude case, so that crack growth is less inhibited. For example, if the plastic zone diameter D^i in Figure 3.4 was caused by so large a load that,

$$\Delta a + D^i > D_{OL} \qquad (3.34)$$

This would result in a crack growth acceleration for the applied cycle. Then, K_{red} will have a negative value. This model uses an acceleration adjustment term ϕ_A, for K_{red} defined as,

$$\phi_A = (1-R_L) \qquad (3.35)$$

where R_L adjusts the magnitude of acceleration depending on the ratio of the current underload stress to the overload stress. Thus residual stress intensity used in eq. 3.24 is defined as

$$K_R = \phi_A \ K_{red} \quad if \ K_{red} < 0 \qquad (3.36)$$

3.3.3 Underload Effects

If a rather significant compressive load which is lower than the most previous minimum load occurs, this load is defined as "underload", σ_{UL}, as in Figure 3.5. In the model negative stresses are assumed to negate the crack growth

retardation caused by previous tensile overloads.

The model accounts for underload effect by reducing the effective overload stress intensity factor, K^*_{max}, eq 3.30, by using the ratio,

$$\beta = \frac{K_{pr} - K_{UL}}{K^*_{max} - K_{UL}} \qquad (3.37)$$

where K_{pr} and K_{UL} are defined in Figure 3.5.

Thus a new effective stress intensity factor, denoted K'_{OL}, is introduced such that

$$K'_{OL} = \frac{K^*_{max}}{Z - Y}(Z - \beta) + K_{max} \qquad (3.38)$$

where Z is the value of β above which K'_{OL} is equal to K_{max}, and Y is the value of β below which K'_{OL} is equal to K^*_{max}. The relationship among these variables is shown in Figure 3.7.
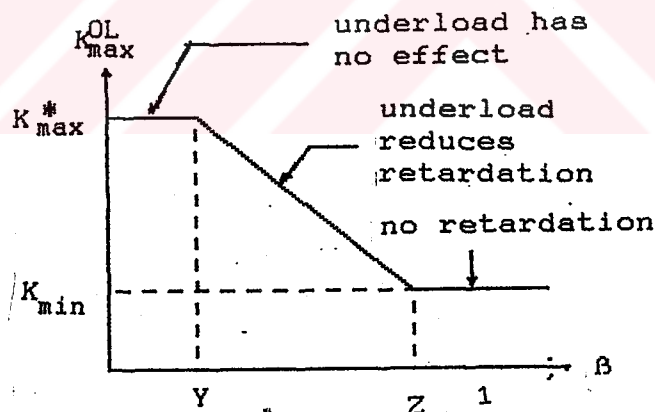
Figure 3.7: Schematic of underload effects [26]

3.4 GENERALISED WILLENBORG MODEL BY CHANG [27]

This model uses a modified Walker equation for effective stress ratio values greater than zero.

for the case of $R_{eff} > 0$

for $\Delta K > \Delta K_{TH}$

$$\frac{da}{dN} = C \left[\frac{\Delta K}{(1-R_{eff})^{1-m}} \right]^n \tag{3.39}$$

$$if \begin{pmatrix} R_{eff} < R_{cut}^+ & , & R_{eff} = R_{eff} \\ R_{eff} \geq R_{cut}^+ & , & R_{eff} = R_{cut}^+ \end{pmatrix}$$

for $\Delta K < \Delta K_{TH}$

$$\frac{da}{dN} = 0 \tag{3.40}$$

$$\Delta K_{TH} = (1-R) \Delta K_{TH_0} \tag{3.41}$$

where m is the Walker stress ratio layer collapsing factor.

The model uses the Willenborg residual stress intensity factor, K_{red} to calculate the effective stress.

$$K_{red} = K_{max}^* - K_{max} \tag{3.42}$$

$$K_{red} = K_{max}^{OL} \quad (-\Delta a \ D_{OL} \quad - K \tag{3.43}$$

then.

$$K_{maxeff} = K_{max} - \Phi K_{red} \tag{3.44}$$

$$K_{mineff} = K_{min} - \Phi K_{red} \qquad (3.45)$$

where D_{OL} is plastic zone radius, such that

$$D_{OL} = \frac{1}{6\pi} \left(\frac{K_{max}}{\sigma_{YS}}\right)^2 \quad \textit{for plane strain} \qquad (3.46)$$

$$D_{OL} = \frac{1}{2\pi} \left(\frac{K_{max}}{\sigma_{YS}}\right)^2 \quad \textit{for plane stress} \qquad (3.47)$$

and the multiplier, Φ is given by

$$\Phi = \frac{[1 - (K_{TH_0}/K_{max}^{OL})]}{S-1} \qquad (3.48)$$

where S is the shut-off ratio (K^{OL}_{max} / K_{max}). For this model the selection of the shut-off ratio is important. Careless selection of S may lead to some 20% error in predictions.

The effective stress range and effective stress ratio are defined as

$$\Delta K_{eff} = K_{maxeff} - K_{mineff} = \Delta K \qquad (3.49)$$

$$R_{eff} = \frac{K_{mineff}}{K_{maxeff}} \qquad (3.50)$$

Note that the effective stress intensity factor range ΔK_{eff} has the same value as ΔK. This model predicts the crack growth retardation by reducing effective stress ratio below that remotely applied.

<u>for the case $R_{eff} < 0$</u>

For the compressive load acceleration, the following equation is used,

$$\frac{da}{dN} = C \left[K_{maxeff}(1-R_{eff})^q \right]^n \qquad (3.51)$$

$$if \begin{pmatrix} R_{eff} > R_{cut}^- & , & R_{eff} = R_{eff} \\ R_{eff} \leq R_{cut}^- & , & R_{eff} = R_{cut}^- \end{pmatrix}$$

This equation is similar to eq.3.39 in the mathematical form, but the exponent, q, is considered as the negative stress ratio index which does not act as the Walker's stress ratio layering factor m does in eq.1. For a specific stress ratio (R < 0), q is determined by,

$$q = \frac{[\frac{\ln(r)}{\ln(1-r)}]}{n} \qquad (3.52)$$

where r is the ratio of the crack growth rate at a specific negative stress ratio to its R=0 counterpart.

The model accounts for the reduction of the tensile overload retardation effects caused by the compressive load immediately following the tensile overload by applying an effective overload retardation zone size, given as

$$D_{eff}^{OL} = (1+R_{eff})D_{OL} \quad , \quad R_{eff} < 0 \qquad (3.53)$$

3.5 EVALUATION OF YIELD ZONE MODELS

Yield zone models, proposed in early 70's such as Willenborg, Wheeler, only accounted for retardation effects. Since then it has been shown that various load interaction effects (crack growth acceleration, underload) have significant effects on spectrum crack growth. The above discussed modified versions of these early models introduce some parameters that account for these load interaction effects. The Willenborg / Chang model accounts for overload retardation, compressive load acceleration effects and reduction of overload retardation effects by compressive loads immediately following tensile overloads. Multi Parameter Yield Zone Model accounts for overload retardation, acceleration due to current overloads and underloads resulting in a reduction of the retardation effects of an overload and multiple overload effects.

Even though these models, especially modified versions, sometimes give good correlations with respect to crack growth data, they are unrealistic in regard to real crack growth mechanisms. For this reason they use for every observable phenomenon a material dependent parameter, leading to high costs in supplying material properties with a mean predictive capacity.

IV. CHARACTERISTIC-K CONCEPTS

This approach involves finding a characteristic-K value that can be correlated to fatigue crack growth rates of a variable amplitude loading [29,30,31,32]. Namely, replacement of a load history of variable amplitude by an equivalent loading such that if applied as a constant amplitude loading the same fatigue life is obtained.

4.1 THE ROOT-MEAN-SQUARE (RMS) METHOD [29]

To predict variable amplitude loading crack propagation, the RMS method assumes that crack growth rates obtained in CA loading with rms-maximum and rms-minimum stress levels is equal to variable amplitude crack growth rates.

For rms-stress values the following relationship is given

$$\sigma_{max_{rms}} = [\frac{1}{m} \sum_{i-1}^{m} (\sigma_{max})^2]^{\frac{1}{2}} \qquad (4.1)$$

$$\sigma_{min_{rms}} = [\frac{1}{m} \sum_{i-1}^{m} (\sigma_{min})^2]^{\frac{1}{2}} \qquad (4.2)$$

where σ_{max} and σ_{min} are respectively the maximum and minimum stresses obtained from the load spectrum . After the calculation of σ_{maxrms} and σ_{minrms}, the rms-ratio, R_{rms}, may be calculated using

$$R_{rms} = \frac{\sigma_{min_{rms}}}{\sigma_{max_{rms}}} \qquad (4.3)$$

The maximum and minimum stress intensity factors are given by

$$K_{max} = Y \cdot \sigma_{max_{rms}} \sqrt{\pi a} \qquad (4.4)$$

$$K_{min} = Y \cdot \sigma_{min_{rms}} \sqrt{\pi a} \qquad (4.5)$$

where Y is the correction on the effect of the finite specimen width. The rms stress intensity range is calculated from,

$$\Delta K_{rms} = K_{max_{rms}} - K_{min_{rms}} \qquad (4.6)$$

To predict crack growth, the Forman equation

$$\frac{da}{dN} = \frac{C (\Delta K_{rms})^n}{(1-R_{rms}) K_c - \Delta K_{rms}} \qquad (4.7)$$

is used.

4.2 EQUIVALENT LOADING APPROACH [30]

The model uses the Paris Law for crack growth predictions. If the number of load cycles is N, the average crack growth rate will be, (ignoring interaction effects)

$$\Delta a_i = C \left[f\left(\frac{a}{w}\right) \Delta\sigma^i \sqrt{a} \right]^n \qquad (4.8)$$

$$\frac{da}{dN} = C \left[f\left(\frac{a}{w}\right) \sqrt{a} \right]^n \left[\frac{1}{N} \sum (\Delta\sigma_i)^n \right] \qquad (4.9)$$

The equivalent constant amplitude loading $\Delta\sigma_{eq}$ which would produce this crack growth rate would be

$$\frac{da}{dN} = C \left[f\left(\frac{a}{w}\right) \sqrt{a} \right]^n \left[\Delta\sigma_{eq} \right]^n \qquad (4.10)$$

where,

$$\Delta\sigma_{eq} = \left[\frac{1}{N} \sum (\Delta\sigma_i)^n \right]^{\frac{1}{n}} \qquad (4.11)$$

where n is the exponent of the Paris Law. The equivalent constant amplitude loading is the statistical moment of nth order of the sequence.

In particular when n is equal to 2, the equivalent loading is the second order of the sequence which is also called the root-mean-square value of the sequence.

4.3 Evaluation of the Characteristic-K Concept

A necessary condition for the applicability of this kind of approach is stationary crack growth behaviour. The concept can not be applied to a load spectrum which contains many discrete events or rare loads. On the other hand, these models have some advantages as to simplicity , computation time and costs. For stationary spectra they give reasonable accuracy.

The Two models, discussed above, differ from each other with regard to the statistical moment of the load sequence. The RMS value has been used not because there is a theoretical justification for it, but because it is a widely used statistical parameter in the analysis of random processes. Therefore, taking the statistical moment (n) as the exponent of the Paris Law may improve predictions.

V. STRIP YIELD MODELS

These models are based on the Dugdale model for calculating the plastic zone size. In order to understand how these models work, first the Dugdale strip yield model will be reviewed.

5.1 Dugdale Strip Yield Model

The model is only valid for large plates in plane stress state and for elastic perfectly plastic materials. Dugdale argued that a crack of length 2a plus the plastic zones at both tips of length D can be obtained by the superposition of two simple separate cases; a crack of length $2l=2a+2D$ subject to remote stress σ plus a crack of length $2l=2a+2D$ subject to $\sigma=\sigma_{YS}$ along the crack faces at both tips, representing the strip yield regions (Figure 5.1).
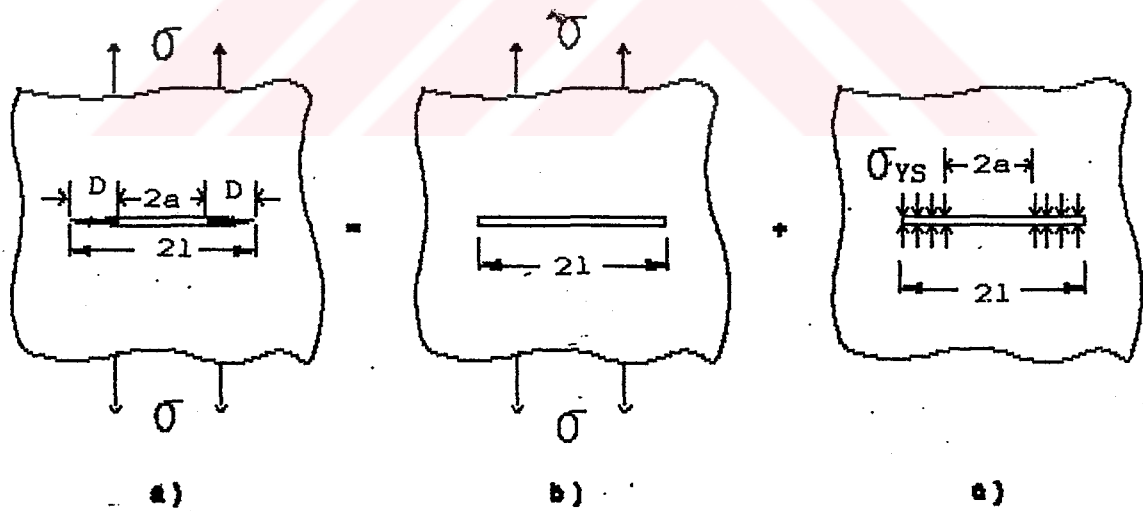
Figure 5.1: The Dugdale model (a) as a superpsition of two simple cases (b) and (c) [8].

The stress intensity at the end of the plastic zone must be zero, that is, the plastic zone D must be of such a length that K due to remote stress σ equals the K due to σ_{YS} on faces of the crack.

For Figure 1(b) :

$$K = \sigma \sqrt{\pi l} \qquad (5.1)$$

For Figure 1(c) :

$$K = 2\sqrt{\frac{l}{\pi}} \; \sigma_{YS} \, \arccos\frac{a}{l} \qquad (5.2)$$

thus

$$\sigma\sqrt{\pi l} = 2\sqrt{\frac{l}{\pi}} \; \sigma_{YS} \, \arccos\frac{a}{l} \qquad (5.3)$$

gives

$$\frac{D}{l} = 2 \, \sin^2\left(\frac{\pi}{4}\frac{\sigma}{\sigma_{YS}}\right) \qquad (5.4)$$

For $\sigma/\sigma_{YS} \ll 1$, $\sin x = x$ leads to

$$D = \frac{\pi}{8}\left(\frac{K}{\sigma_{YS}}\right)^2 \qquad (5.5)$$

5.2 NEWMAN'S CRACK CLOSURE MODEL [33]

The model uses the crack growth rate equation proposed by Hardrath which includes low growth rates approaching threshold and high growth rates approaching fracture.

$$\frac{da}{dN} = C \, (\Delta K_{eff})^n \; \frac{1-(\frac{\Delta K}{\Delta K_{eff}})^2}{1-(\frac{K_{max}}{K_c})^2}$$ (5.6)

where,

$$\Delta K_o = C_1 \, (1-C_2 \frac{\sigma_{op}}{\sigma_{max}})$$ (5.7)

$$K_{max} = Y. \, \sigma_{max} \, \sqrt{\pi a}$$ (5.8)

$$\Delta K_{eff} = Y. \, (\sigma_{max}-\sigma_{op}) \sqrt{\pi a}$$ (5.9)

The coefficients C_1 and C_2 are determined from the threshold stress intensity factor range.

The assumption made in Newman's strip yield model is that crack opening in the plastic zone (a<x<l) (see Figure 5.1) is accommodated by plastic elongation in the plastic strip. The COD is assumed to become the vertical length of plastic material. In other words, elastic crack opening of the fictitious crack tip is supposed to equal the plastic deformation in the real crack tip zone. The crack will now grow into a plastic zone with a quantified plastic elongation. The result is that the plastically deformed material is left in the wake of the crack. Upon unloading, this should lead to crack closure at a positive stress. Figure 5.2 shows a schematic of the model at maximum and minimum applied stress. the crack is composed of three regions (1) a linear elastic region outside

the plastic zone of the crack (2) a plastic region of length D at the crack tip and (3) a residual plastic deformation region along the crack surfaces. Region (2) and (3) are composed of rigid-perfectly plastic bar elements with a flow stress σ_0 . At any applied stress , the bar element are either intact or broken. The broken elements carry compressive loads only, and only if they are in contact with each other. To account for the effects of the state of stress on plastic zone size a constraint factor (α) is used to elevate the tensile flow stress for the intact elements in the plastic zone. The upper and lower bounds for α is 1 under plane stress and 3 under plane strain , respectively, leading to σ_0 and $3\sigma_0$

a) Maximum stress   b) Minimum stress
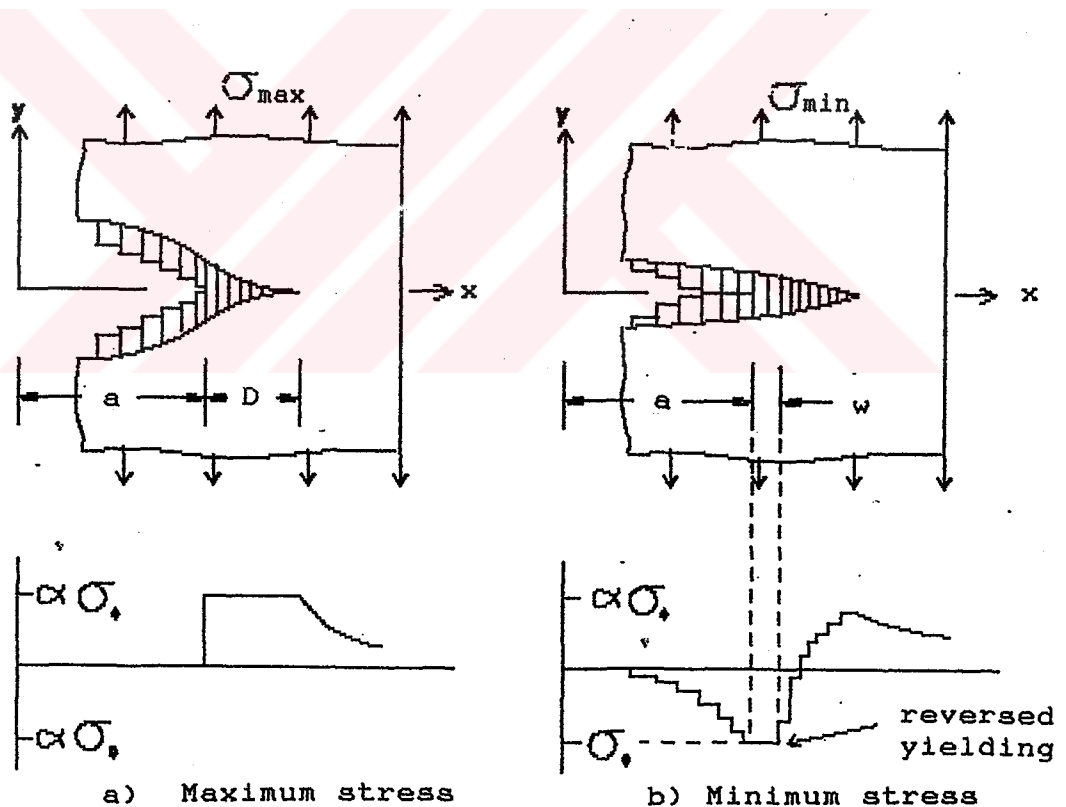
Figure 5.2: Crack surface displacements and stress distributions along crack line [33]
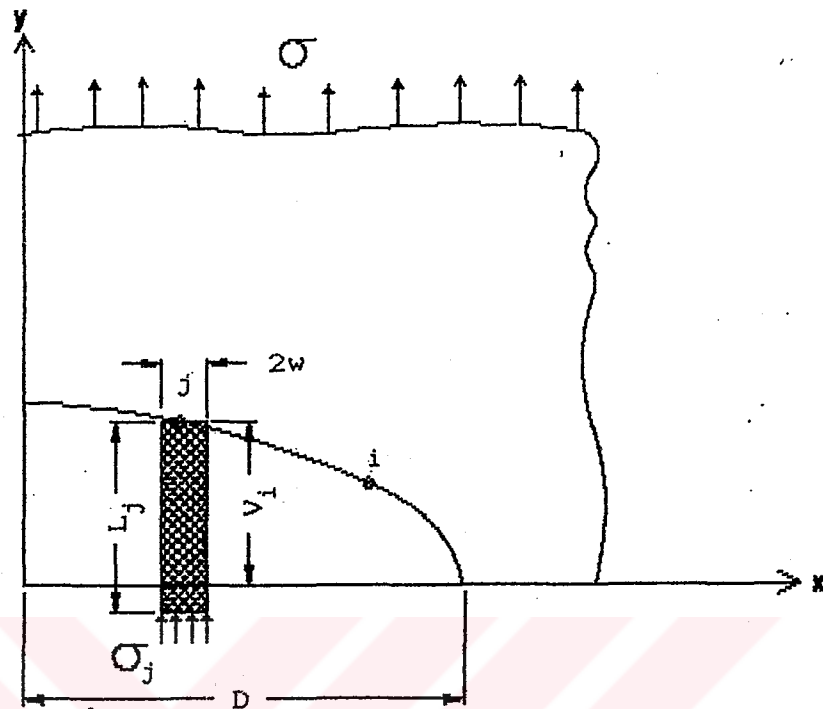
Figure 5.3: Schematic of loading and coordinate
system used in the model [33]

Figure 5.3 shows a breakdown of the components of the
model and the coordinate system used for one quarter of the
plate. The plate has a fictitious crack of half length l and is
subjected to a uniform stress σ. The bar element is in contact
when the length of the element (L_j) is larger than the current
crack surface displacement (V_j). The equations that govern the
response of the system were obtained by requiring that
compatibility be met between the elastic plate and all of the
bar elements along the crack surface and plastic zone boundary.
The displacement at point i is

$$V_i = \sigma \, f(x_i) - \sum_{j=1}^{n} \sigma_j \, g(x_i, x_j)$$

(5.10)

where n is the number of the bar elements and $f(x_i)$, $g(x_i, x_j)$ are influence functions. The bar elements at point i have a length of L_i . The compatibility equation ($V_i = L_i$) is expressed as

$$\sum_{j=1}^{n} \sigma_j \; g(x_i, x_j) \; = \; \sigma \; f(x_i) - L_i \qquad (5.11)$$

5.2.1 Plastic Zone Size and Approximations

The plastic zone size, D, is given as

$$D = a \; [[\frac{W}{\pi a} \; \sin^{-1}[\; \sin(\frac{\pi a}{W}) \; \sec(\frac{\pi \sigma_{max}}{2\alpha\sigma_0}) \;] -1] \qquad (5.12)$$

In the model, the plastic zone size is arbitrarily divided into ten bar elements. The aspect ratios ($2w_i$/D) are 0.01, 0.01, 0.02, 0.04, 0.06, 0.09, 0.12, 0.15 and 0.3. The smallest elements are located near the crack tip (x=a). At maximum applied stress the plastic zone size is calculated from eq.5.12. L_i changes by plastic deformation only when an element yields in tension ($\sigma_j > \alpha\sigma_0$) or compression ($\sigma_j < -\sigma_0$).

5.2.2 Contact Stresses at Minimum Load

When unloaded to a minimum load (Figure 2b), some of the elements near the crack tip will yield in compression ($\sigma_j < -\sigma_0$). The Compressive plastic zone (w) varies from one tenth to one half of the plastic zone (D), depending on the amount of closure and constraint factor. The elements along the crack surfaces, which store residual deformation, may come into contact and carry compressive stresses. Some of these elements may yield in compression. The stresses in the plastic zone and the contact stresses along the crack surfaces are calculated from eq.5.11 with $\sigma = \sigma_{min}$. For elements that yield in compression, σ_i is set equal to ($-\sigma_0$) and the length of the

elements are set equal to the final displacements at those points, that is

$$L_i - V_i - \sigma_{min} \; f(x_i) - \sum_{j=1}^{n} \sigma_j \; g(x_j, x_i)$$ (5.13)

For elements not in contact ($L_i < V_i$), $\sigma_i = 0$

5.2.3 Crack Opening Stresses

σ_{op} is calculated from the contact stresses at σ_{min}. To have no surface contact, the stress intensity factor due to an applied stress increment $(\sigma_{op} - \sigma_{min})$ is set equal to the stress intensity factor due to contact stresses.

5.2.4 Crack Extension and Approximations

Apparently cycle-by-cycle calculation of σ_{op} would require most extensive computer time, while reassessments of the number and location of bar elements would also be problematic. To avoid these problems Newman assumed that σ_{op} remains constant during a small crack extension arbitrarily defined as

$$\Delta a = 0.05 \; D_{max}$$ (5.14)

where D_{max} is the plastic zone size when the maximum stress is applied.

Crack growth may then be calculated cycle-by-cycle using eq.5.1. The calculation is continued either until a crack extension equal to Δa in eq.5.14 has been reached or until 300 cycles have been applied. When using the model the constant σ_{op} is calculated by considering the load cycle with highest σ_{max} in the period considered and the lowest σ_{min} before and after the occurrence of that σ_{max} value. The procedures are then repeated for the next interval Δa.

5.3 Evaluation of Strip Yield Models

Strip yield models are generally very successful in calculating crack opening stresses and predicting crack growth rates, but the models are very complex. Iterative solution procedures have to be used, resulting in a heavy computer load for cycle-by-cycle calculations. In this respect some simplifying assumptions and approximations should be introduced, such as holding σ_{op} and Y constant during crack growth increment Δa, leading to some lost sequence and interaction effects. Another drawback is that the models are applicable only to the plane stress condition. Newman introduced a plastic constraint factor (α) to account for plane strain. But suitability of a constraint factor is questionable, as the Dugdale model is valid only for plane stress conditions and the constraint factor is not constant during spectrum loading.

VI. NON-INTERACTION MODELS

This approach assumes the crack growth increment in each cycle to be independent of previous load history. The models involve cycle-by-cycle integration of crack growth increments using crack growth laws, which may or may not include crack closure.

The assumption of non-interaction is obviously incorrect. In general, non-interaction predictions of crack growth under variable amplitude loading will be conservative, but they can easily be overly conservative. Also, they can not be relied on to predict the correct trends of variations in spectrum and test parameters. On the other hand, computational efficiency and the availability of extensive data bases for constant amplitude fatigue crack growth that includes various crack geometries are certain advantages. For further understanding a representative model will be discussed.

6.1 HALF-CYCLE METHOD [34]

This method uses the Walker equation for fatigue crack growth.

$$\frac{da}{dN} = C \ (K_{max})^{n} \ (1-R)^{m} = C \ (\Delta K)^{n} \ (1-R)^{m-n} \qquad (6.1)$$

The half-cycle theory states that the damage (or crack growth) caused by each half-cycle of either increasing or decreasing load is assumed to equal one half the damage caused by a complete cycle of the same loading magnitude (ΔK,R). As shown in Figure 6.1. random stress cycles are divided into two phases of increasing and decreasing loads (Figure 1b). Each half cycle is considered a complete cycle. The crack growth caused by each is calculated separately according to equation 6.1. The result is divided by two to find the real crack growth. That is

$$\Delta a_i = \frac{\Delta a_{i,1} + \Delta a_{i,2}}{2} \qquad (6.2)$$

$$a_i = a_{i-1} + \frac{\Delta a_{i,1} + a_{i,2}}{2} \qquad (6.3)$$

where $\Delta a_{i,1}$ is the calculated growth using ascending part of the load cycle i, $\Delta a_{i,2}$ is the calculated growth using descending part of the load cycle i, and

$$\Delta a_i = C \left(\Delta K_{i,1}\right)^n (1-R)^{m-n} + C \left(\Delta K_{i,2}\right)^n (1-R)^{m-n} \qquad (6.4)$$
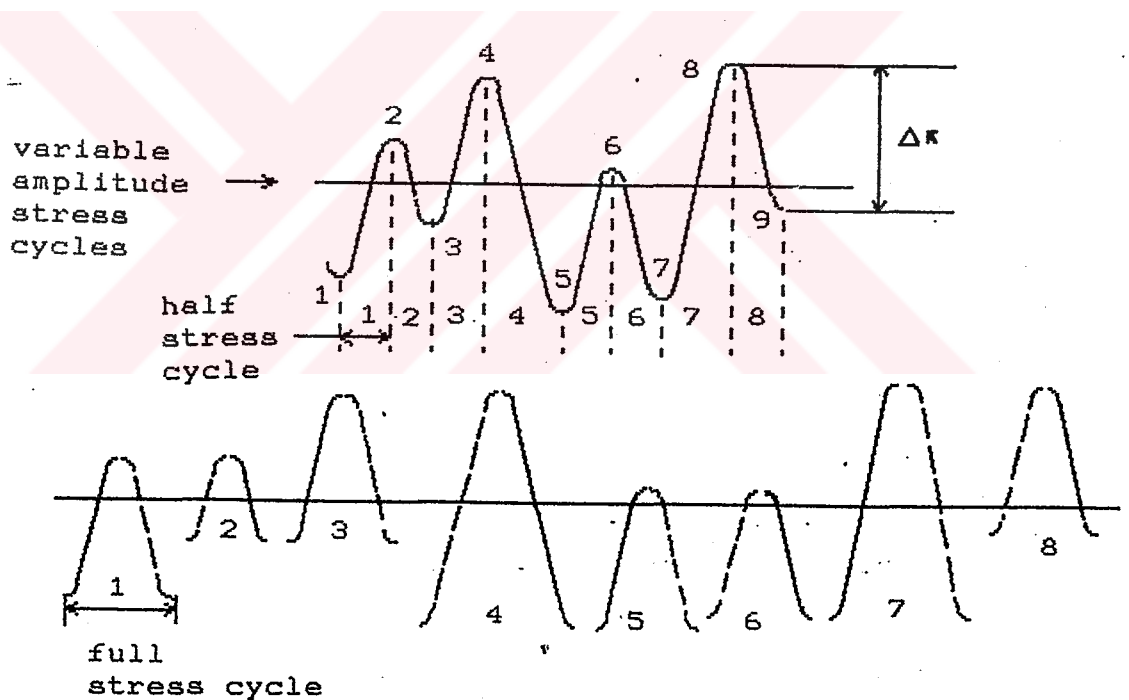
Figure 6.1: Resolution of random stress cycles into half stress cycles of different stress ranges [34]

VII. CRACK OPENING MODELS

7.1 INTRODUCTION

The crack opening models include crack closure as the basic mechanism to account for interaction effects [10,35,36,37]. They are based on the assumption that crack growth occurs during the period when the crack is open. The cycle-by-cycle crack growth concept leads to cycle-by-cycle calculation and readjustment of the crack opening stress level (σ_{op}). Even though this may lead to heavy calculations the predictions can still be made in a relatively short time compared to the strip yield models.

In this section two models, PREFFAS and ONERA, will be discussed. In the next section, a detailed analysis of the CORPUS model will be given. If we consider the common aspects of these models, σ_{op} and the corresponding K_{op} should be calculated cycle-by-cycle which leads to an effective stress intensity range for the subsequent cycles.

$$\Delta K_{eff} - K_{max}^i - K_{op}^i \qquad (7.1)$$

Crack growth data obtained under constant amplitude are then adapted in the following format.

$$\frac{da}{dN} - f(\Delta K_{eff}) \qquad (7.2)$$

It is thus assumed that the same ΔK_{eff} under constant amplitude loading and under variable amplitude loading will produce the same crack extension (similitude concept). In all three models it is recognised that K_{op} will heavily depend on high positive peak loads and high negative peak loads.

7.2   THE PREFFAS MODEL

The PREFFAS Model was proposed by Aliaga, Davy and Schaff [36,37].   It is a simple model requiring easy calculations with a few crack growth calibration tests to characterize the material response and its sensitivity to overload effects.

7.2.1   Crack Growth Law

The crack growth at cycle i is given as

$$\Delta a^i - C\ (K_{max}^i - K_{op}^i)\tag{7.3}$$

There are no threshold considerations. The model predicts crack growth even if (K_{max}^i - K_{op}^i) is lower than ΔK_{th}.

7.2.2   Selection of Opening Point

To find the crack opening stress K_{op}^i of cycle i, all important cycles that can determine K_{op}^i should be considered. If $K_{op}^i{}^j$ is the opening stress intensity factor at cycle i induced by cycle j, $K_{op}^i{}^j$ can be found by using K_{max}^j and K_{min}^k, which is the minimum value of K of cycles that are between cycles j and i (Figure 7.1).

$$K_{max}^i - K_{op}^{ij} - U(K_{max}^j - K_{min}^k)\tag{7.4}$$

$$1 - \frac{K_{op}^{ij}}{K_{max}^j} - U(1-R)\tag{7.5}$$
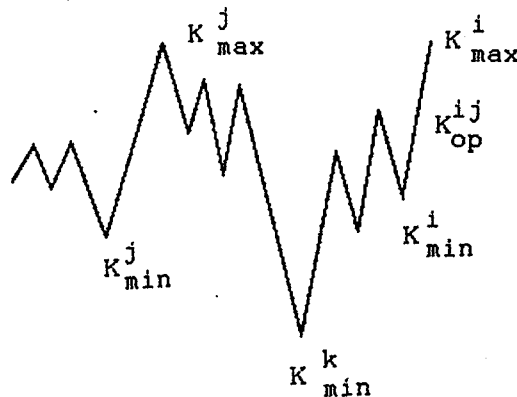
Figure 7.1: Selection of Opening Points [36]

$$K_{op}^{ij} = K_{max}^{j}(1-U+UR) \qquad (7.6)$$

where

$$R = \frac{K_{min}^{k}}{K_{max}^{j}} \qquad (7.7)$$

$$U = A+BR \qquad A,B \ material \ properties \qquad (7.8)$$

Finally, to find the opening stress of cycle i (K_{op}^{i}), every cycle before the cycle i induces an opening stress intensity $(K_{op}^{i\,j})$ and the cycle that induces the greatest opening stress intensity $(K_{op}^{i\,j})$ determines K_{op}^{i} that is,

$$K_{op}^{i} = \max(K_{op}^{ij})_{j=1}^{j=i-1} \qquad (7.9)$$

and K_{op}^{i} is used to predict the crack growth at cycle i.

7.2.3 The History Values

It is not necessary to calculate opening stress intensity of every cycle $(K_{op}^{i\,j})$ that occur before the cycle i. Only significant values referred to as history values are designated KH and must be memorized (Figure 7.2).

These values are strictly in the following form

$$KH_{max}^{r-2} \succ KH_{max}^{r-1} \succ KH_{max}^{r} \Big] \; with \; KH_{op}^{r-2} \prec KH_{op}^{r-1} \prec KH_{op}^{r}$$
$$KH_{min}^{r-2} \prec KH_{min}^{r-1} \prec KH_{min}^{r}$$

KH_{op} values are found according to eq. 7.6. From this history values, eq. 7.9 becomes

$$K_{op}^{i} - \max(K_{op}^{ij})_{j-1}^{j=i-1} - KH_{op}^{r} \qquad (7.10)$$

where r is the latest history value.

Figure 7.2 shows schematically how the model works. In the case of Figure 7.2a, the rank is three. If there is a load point lower than r-1, 3rd will be erased and the opening stress intensity induced by the second history cycle on the current cycle should be updated. If KH_{op}^{2} is still greater than KH_{op}^{1}, the opening stress will be, according to eq 7.10 (Figure 7.2)

$$K_{op}^{i} - KH_{op}^{r} - KH_{op}^{2} \qquad (7.11)$$

In this case rank is lowered to two. If another load level which is lower than KH_{min}^{2} is applied (Figure 7.2c), then

$$K_{op}^{i} - KH_{op}^{r} - KH_{op}^{1} \qquad (7.12)$$

In which case, the rank is lowered to one.

According to the degree of the underload earlier history values of KH_{max} can be used. This is why earlier history values should be kept in memory.

7.2.4 Calculation of Sequence Efficiency (EF)

The sequence efficiency is the summation of the effective stress ranges of all load cycles in one block of the load spectrum.

The effective stress range is calculated cycle-by-cycle.
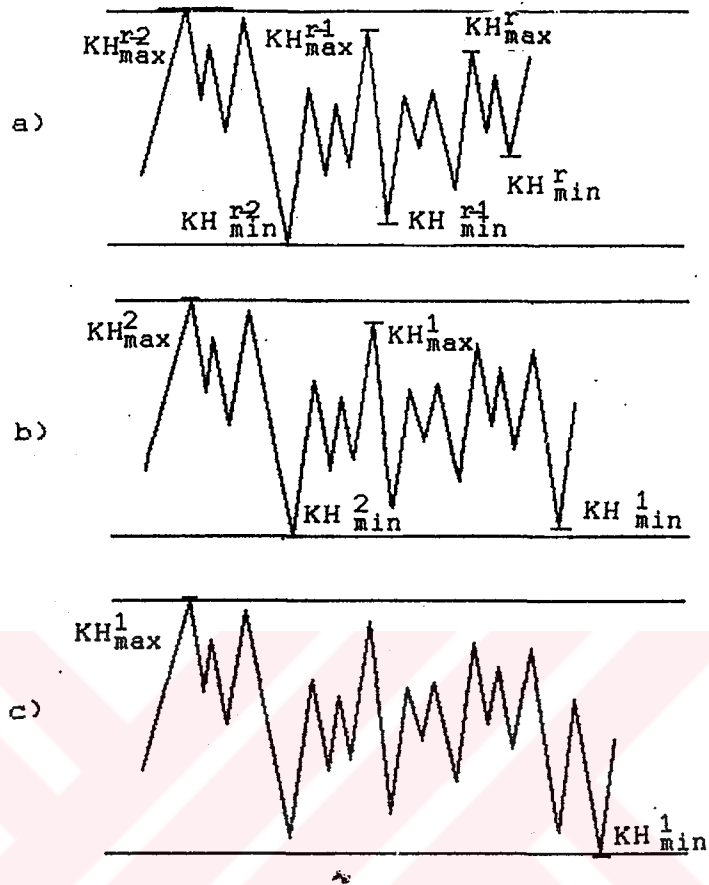
Figure 7.2: History values and their modification with application of new loads

$$EF = \sum_{i=1}^{m} (\Delta\sigma^{i}_{eff})^{n} \qquad (7.13)$$

If $\sigma^{i}_{max} < \sigma H^{r}_{max}$

With σ^{i}_{max} and σ^{i+1}_{min}, the KH series must be updated to satisfy the condition imposed on the KH series defined earlier.

Modification occurs, if,

a. $\sigma^{i+1}_{min} < \sigma H^{r}_{op}$ (underload effect, which has been discussed (see Figure 7.2c))

b. $\sigma_{op} > \sigma H^{r}_{op}$ (This means introduction of an additional level in the KH series).

If $\sigma^{i}_{max} > \sigma H^{r}_{max}$

It is, not possible to make cycle-by-cycle counting conservative when a large stress variation is obtained through

several small amplitude cycles. In the model a modified rain-flow counting method is used (Figure 7.3) to overcome this difficulty. It can be seen that the value of σ^i_{max} eliminates local retardation effects caused by σH^r_{max} (since $\sigma^i_{max} > \sigma H^r_{max}$) and the calculation based on the earlier history value σH^{r-1}_{op} would therefore give a larger growth value. In that case, the model uses the earlier opening point, that is

$$\Delta a^i = C[(\sigma^i_{max} - \sigma H^{r-1}_{op})^n + (\sigma H^r_{max} - \sigma H^r_{op})^n - (\sigma H^r_{max} - \sigma H^{r-1}_{op})^n] \quad (7.14)$$
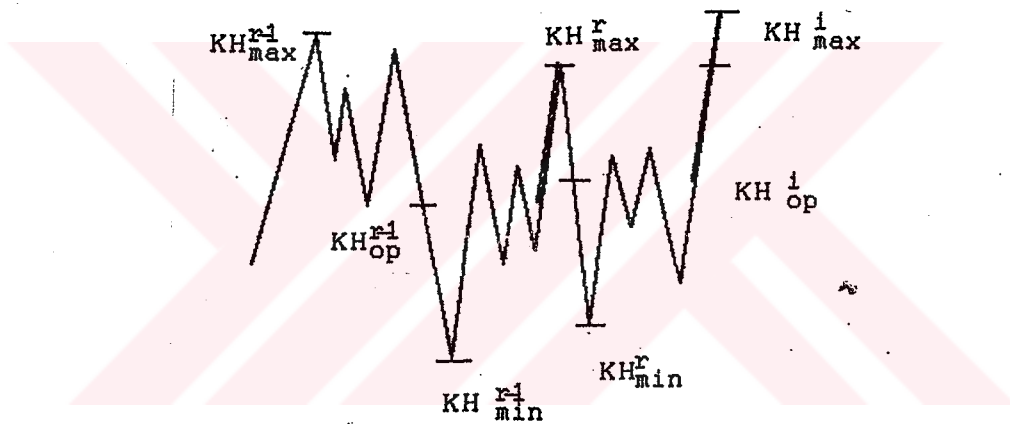
Figure 7.3: Rain-flow effect [36]

where $(\sigma^i_{max} - \sigma H^{r-1}_{op})$ is like a typical rain-flow part and $(\sigma H^r_{max} - \sigma H^{r-1}_{op})$ which, represents a crack growth calculated before cycle i, must be subtracted (Figure 7.3). Figure 7.4 and 7.5 show how the load cycles are be transformed by the rain-flow approach.

7.2.5 Crack Growth Calculation

In the PREFFAS model, the crack length for the calculations of K values is assumed to be constant within a block of a flight load spectrum. Δa, the crack growth increment
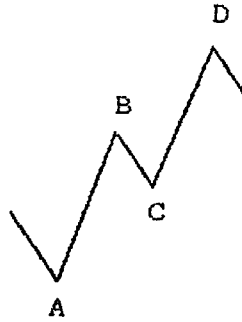
Figure 7.4: Load cycles that can be accounted for
by rain-flow approach
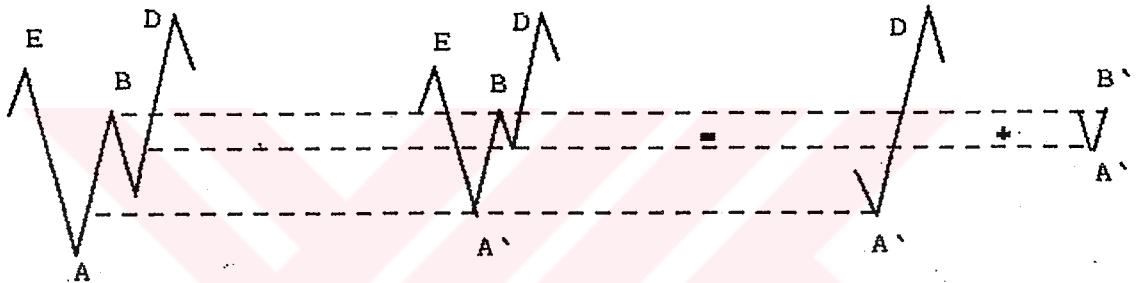
Figure 7.5: Load cycle transformation as a consequence of
the rain-flow approach [7]

in one block of the spectrum, is given by

$$\Delta a - \sum_{i=1}^{m} \Delta a^i - C \sum_{i=1}^{m} (\Delta K_{eff}^i)^n \qquad (7.15)$$

where m is the number of load cycles in one block.

$$\Delta K_{eff}^i - f(a) \, \Delta \sigma_{eff}^i \, \sqrt{\pi a} \qquad (7.16)$$

where f(a) is geometry correction factor. Due to the assumption that the crack length (a) is constant in one block, the above equation can be written as

For subsequent calculations the sequence efficiency (EF) has been defined as

$$\Delta a - C \left[f(a) \sqrt{\pi a} \right]^n \sum_{i-1}^m \left(\Delta \sigma_{eff}^i \right)^n \qquad (7.17)$$

$$EF - \sum_{i-1}^m \left(\Delta \sigma_{eff}^i \right)^n \qquad (7.18)$$

Eq. 7.17 can then be written as

$$\Delta a - C \left[f(a) \sqrt{\pi a} \right]^n EF \qquad (7.19)$$

The average crack growth rate per cycle is

$$\left[\frac{da}{dN} \right]_{av} - \frac{\Delta a}{m} - C \left[f(a) \sqrt{\pi a} \right]^n \frac{EF}{m} \qquad (7.20)$$

The integration of crack growth rate gives the fatigue life as

$$N - \frac{m}{\pi \; C \; EF} \; \frac{1}{W^{(n/2-1)}} \int_{\alpha_o}^{\alpha_r} \left(\frac{\cos \alpha}{\alpha} \right)^{\frac{n}{2}} d\alpha \qquad (7.21)$$

where $\alpha = \pi a / W$ and N is fatigue crack growth life as number of cycles. If n is used as the number of flights in one block, N will then be give the life in number of flights.

In the model four material properties are used C,n,A,B. It has been shown that for aluminum alloys and steels A+B = 1. In this way material properties are lowered to three. These are obtained by conducting two tests, one with CA, the other with intermittent overload.

7.2.6 Evaluation of PREFFAS Model

The model is easy to use and because of the stationary crack·length assumption the calculation time to be saved will be large, especially for short block spectra and long predicted lives. But, for a large block size (TWIST) and a short prediction life there is hardly any saving in time.

In the PREFFAS model compressive stresses are truncated to zero. This is a weak point. PREFFAS predicts that the effect of the ground stress level (σ_{gr}) will be absent for most spectra, which systematically disagrees with test results.

As indicated earlier, retardation effects generated by an overload decays as the crack goes through the yield zone induced by that overload. Neglecting this phenomenon is another weakness of the model.

7.3   THE ONERA MODEL

The model calculates crack extension cycle-by-cycle according to the Paris equation.

$$\Delta a^i - C (\Delta K_{eff}^i)^n \qquad (7.22)$$

The opening stress intensity K_{op} used in cycle i is calculated in the previous cycle [38].

7.3.1   Definition of K_{op}

The crack opening K_{op} level depends on equivalent K_{max} and K_{min} values, where K_{maxeq}^i is affected by high loads and K_{mineq}^i by low loads.

7.3.2   Evaluation of K_{maxeq}

As shown in Figure 7.6, if there is a previous overload, D^* is defined as

$$D^* - a_{OL} + D_{OL} - a^i \qquad (7.23)$$

K_{maxeq} is defined as the stress intensity value that would cause a plastic zone D^*.

But if,

$$D^i > D^* \qquad (7.24)$$

then

$$K_{max_{eq}} - K_{max}^i \qquad (7.25)$$
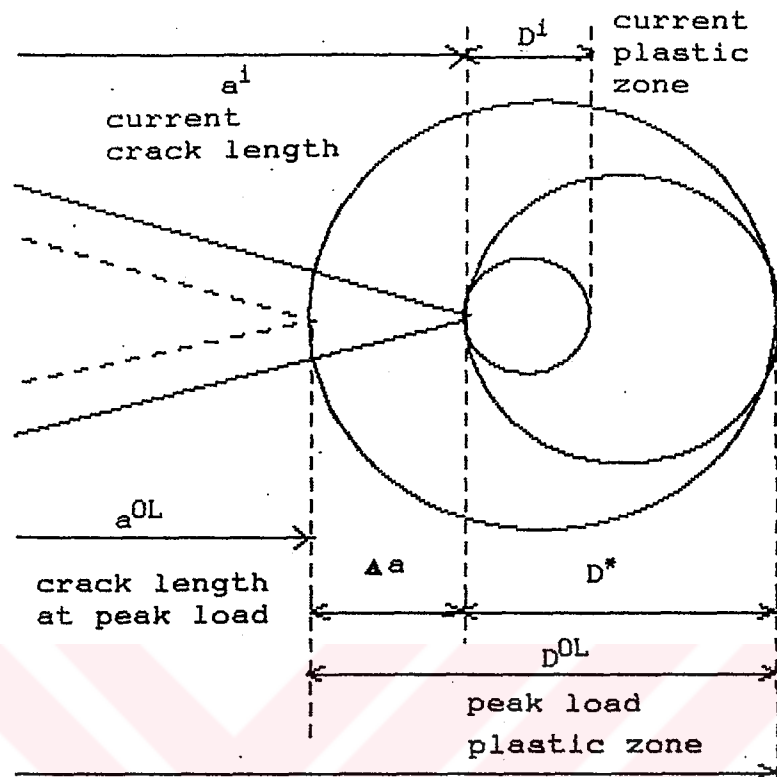
Figure 7.6: Plastic zone after an overload

7.3.3 Plastic Zone Size

In the ONERA model, it is assumed that plane strain/ plane stress plastic zone size ratio is equal to 1/6. At the material surface there is always a plane stress zone. Besides, it is assumed that the size of the plastic zone decreases in the thickness direction following a 45° straight line. As shown in Figure 7.7. The transition between two situations depends on the sheet thickness. It occurs at D = 0.6t. The model adopts the average plastic zone δ_m, which leads to

$$a) \quad \delta_m = \frac{D}{6}\left(1 + \frac{25}{6}\frac{D}{t}\right) \quad if \ D < 0.6t \qquad (7.26)$$

case(a) D < 0.6 t   case(b) D > 0.6t
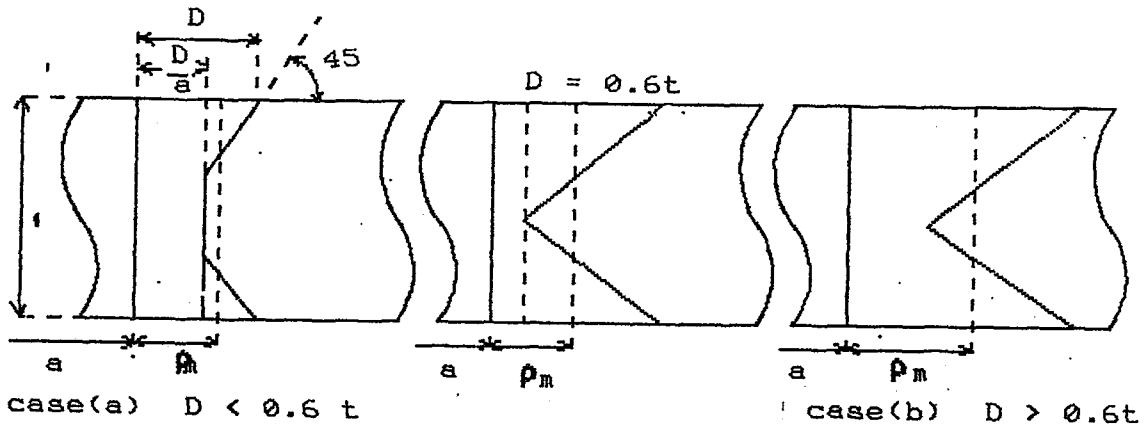
Figure 7.7: Plane strain and plane stress zone diagram [38]

$$b) \quad \delta_m = D - \frac{t}{4} \quad if \geq 0.6t \qquad (7.27)$$

For D, Irwin's formula for plane stress is used

$$D = \frac{1}{\pi} \left(\frac{K}{\sigma_{YS}} \right)^2 \qquad (7.28)$$

and , eq. 7.23 is modified to

$$\delta_m^i = a_{OL} + \delta_m^{OL} - a^i \qquad (7.29)$$

Now, K^i_{maxeq} can be calculated cycle-by-cycle from $D^{*(i)}$ which is derived from δ^i_{eq} by inversion of equations 7.26 and 7.27.

$$\delta_{eq}^{(i)} = 0.12t \left[\sqrt{1 + 100 \frac{\delta_m^i}{t}} - 1 \right] \qquad (7.30)$$

$$\delta^{(i)}_{eq} - \delta^{(i)}_{eq} + \frac{t}{4} \qquad (7.31)$$

then,

$$K^i_{max_{eq}} - \sigma_{YS} \sqrt{\pi \, \delta^{(i)}_{eq}} \qquad (7.32)$$

7.3.4 Evaluation of K_{mineq}

In the model, five different load cases are considered as shown in Figure 7.8.

$$if \quad K^i_{min} < K^{i-1}_{min_{eq}} \qquad (7.33)$$

then, as in the cases of 2 and 3,

$$K^i_{min_{eq}} - K^i_{min} \qquad (7.34)$$

The above equation applies in case 4 where a new monotonic plastic zone is created. In case 1, K^i_{max} doesn't exceed K_{op} and $K_{min} > K_{mineq}$. There will be no change in K_{mineq} and since there is no crack growth, also K_{maxeq} will be the same. However, in the more general case (5) there is plasticity in going to K^i_{max} (although no primary plasticity) and in the reversal of the the load going to K_{min}. Then, it may be expected that both K^i_{max} and K^i_{min} will cause some change of K^i_{mineq}.

$$\Delta K^i_{min_{eq}} - K^i_{min_{eq}} - K^{i-1}_{min_{eq}} \qquad (7.35)$$
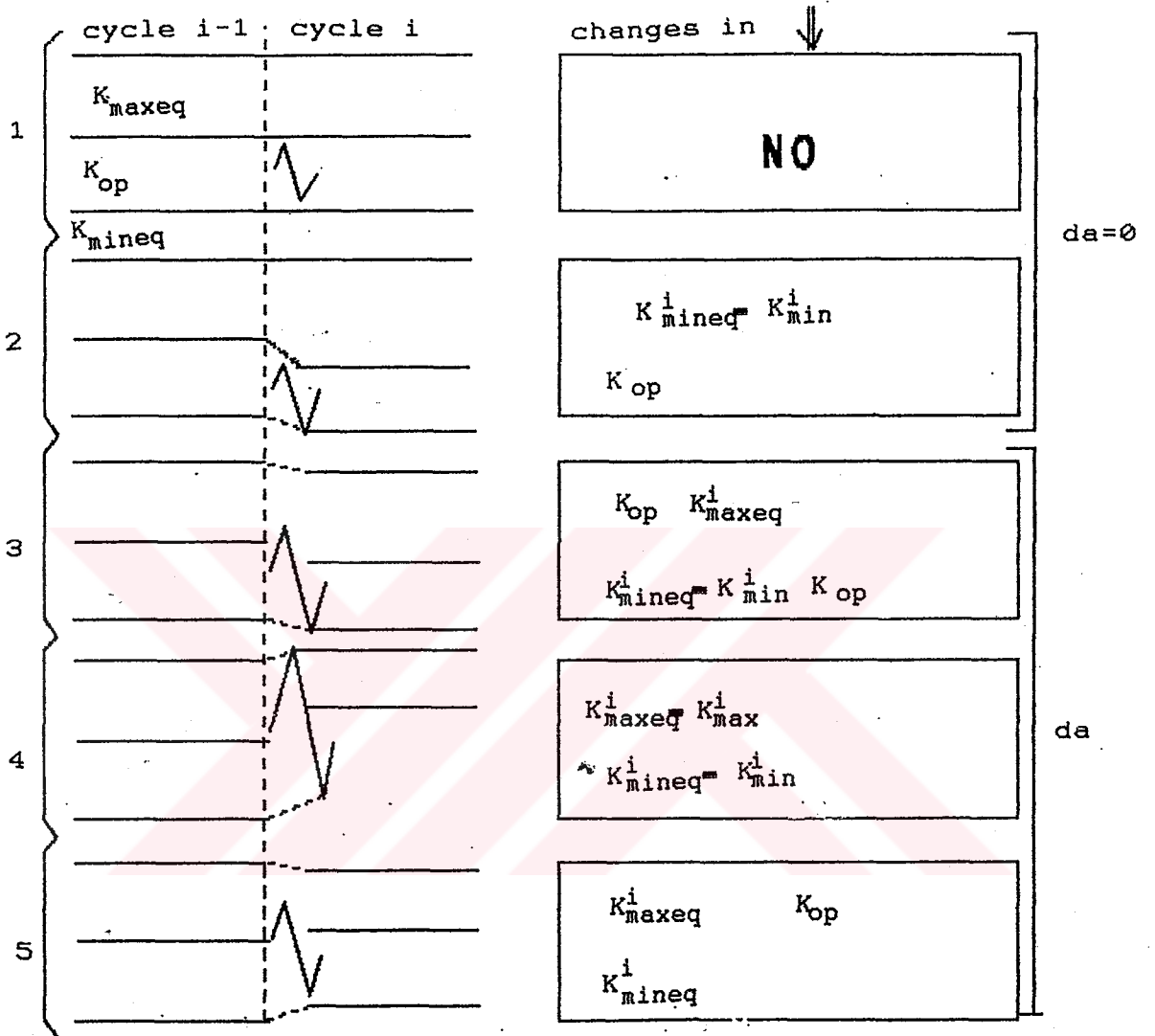
Figure 7.8: Five different Load Cases [38]

It is assumed in the model that this change depends on the ratio,

$$ratio = \frac{K_{max}^{i}}{K_{max_{eq}}^{i}} \qquad (3.36)$$

and the difference,

$$diff - K_{min_{eq}}^{i} - K_{min_{eq}}^{i-1} \qquad (3.37)$$

It is also assumed

$$\Delta K_{min_{eq}}^{i} - diff.ratio^{\beta} \qquad (7.38)$$

where the exponent ß is thickness dependent.

$$\beta - 1 + \frac{t}{2} \qquad (7.39)$$

Eq.7.38 can now be rewritten as

$$K_{min_{eq}}^{i} - diff.ratio^{\beta} + K_{min_{eq}}^{i-1} \qquad (7.40)$$

7.3.5 K_{op} Level

It is postulated in the model that,

$$K_{op}^{i} - K_{max_{eq}}^{i}[\alpha \ f_1 \ R_{eq}^{i} + (1-\alpha) \ f_2 \ R_{eq}^{i}] \qquad (7.41)$$

where,

$$R_{eq}^{i} - \frac{K_{min_{eq}}^{i}}{K_{max_{eq}}^{i}} \qquad (7.42)$$

$$f_1 - 0.377 + 0.623 R_{eq} \qquad if \ R_{eq} > -0.0624 \qquad (7.43)$$

$$f1 = 0.350 + 0.190 R_{eq} \qquad \text{if } R_{eq} < -0.0624 \tag{7.44}$$

$$f_2 = \frac{1}{1.19 - 0.19 R_{eq}} \tag{7.45}$$

f_1 and f_2 are crack opening functions. f_1 is related to the overload case and f_2 is related to the constant amplitude case.

The loading parameter α varies between 0 for CA loading and 1 for a singe overload. It is given as,

$$\alpha = 1 - \frac{1}{M . \sigma'} \sum m(j) \sigma_{max}(j) \tag{7.46}$$

where the peak stress $\sigma_{max}(j)$ occurs $m(j)$ times in the load spectrum. M is the total number of cycles in the load spectrum and σ' is the largest σ_{max} value.

VIII. THE CORPUS MODEL

8.1 Introduction

The CORPUS model was proposed by de Koning [10], [35]. It is the most sophisticated crack opening model, since it includes multiple overload effects, plane stress/plane strain transition, a correction for the effect of high loads on the crack opening stress levels, and the recognition of primary and secondary plastic zones. Crack growth increments are calculated cycle-by-cycle. The model was applied by de Koning to 2 mm aluminum sheet materials ,2024-T3 Alclad and 7075-T6 Clad under F-27 spectra and later by Padmadinata on FALSTAFF,CN-235, TWIST, miniTWIST spectra.

8.2 Fatigue Crack Growth Model

The model is based on a cycle-by-cycle analysis of crack growth, that is

$$a = a_0 + \sum \Delta a_i \qquad (8.1)$$

where Δa_i is the amount of crack growth associated with the load increment $\sigma^i_{max} - \sigma^i_{min}$. It is assumed that growth occurs only in the upward part of the load cycles. Moreover, the growth is a function of effective stress intensity factor ΔK_{eff} given as,

$$\Delta K_{eff} = f(\Delta K_{eff}) \qquad (8.2)$$

The form of the function f is not essential for the model. ΔK_{eff} is given as,

$$\Delta K_{eff} = Y \Delta\sigma^i \sqrt{\pi a} \qquad (8.3)$$

$\Delta\sigma_{eff}$ is specified as,

$$\Delta\sigma^i_{eff} = \sigma^i_{max} - \sigma^i_{min} \qquad if \quad \sigma^i_{op} \leq \sigma^i_{min} \qquad (8.4)$$

$$\Delta\sigma^i_{eff} = \sigma^i_{max} - \sigma^i_{op} \qquad if \quad \sigma^i_{min} < \sigma^i_{op} < \sigma^i_{max} \qquad (8.5)$$

$$\Delta\sigma^i_{eff} = 0 \qquad if \quad \sigma^i_{op} \geq \sigma^i_{max} \qquad (8.6)$$

where σ_{op} stands for the crack opening stress and α is the correction factor accounting for the finite width, given as

$$Y = \frac{1}{\sqrt{1-\left(\frac{a}{b}\right)^2}} \qquad (8.7)$$

The first condition of the equation seems logical, but as a consequence the hump opening function depicted in Figure 8.5, it is impossible that $\sigma^i_{op} < \sigma^i_{min}$. In Figure 8.5, σ_{min} and σ_{op} may be regarded as normalized with respect to σ_{max}. It can be seen that no value of σ_{min} is greater than σ_{op}.

Plasticity effects play an important role on the crack opening and crack closure behaviour.

8.3 Effects of Plastic Deformation on Crack Opening Behaviour

de Koning has explained his hump concept in a qualitative way by considering two plastic effects. Namely, those in front of the crack tip and in the wake of the growing fatigue crack.

Firstly, the effects of plastic deformation in front of

the crack tip are studied. In the analysis the presence of a fictitious initial crack is assumed. This crack has grown at a mean stress level and load amplitude that has left negligible plastic deformations along the crack surface behind it. Then a spike load was applied (Figure 8.1). As a result, plastically deformed material is created at the crack tip. Upon subsequent unloading a zone of material, yielding in reverse is created. Inside this zone the material is loaded additionally from the positive yield limit at the spike load to the negative limit. This implies that with respect to reversed plastic flow the material can carry approximately twice the load increment observed for plastic flow in the virgin material. Therefore the zone of reversed plastic flow is much smaller than the primary zone (Figure 8.2).
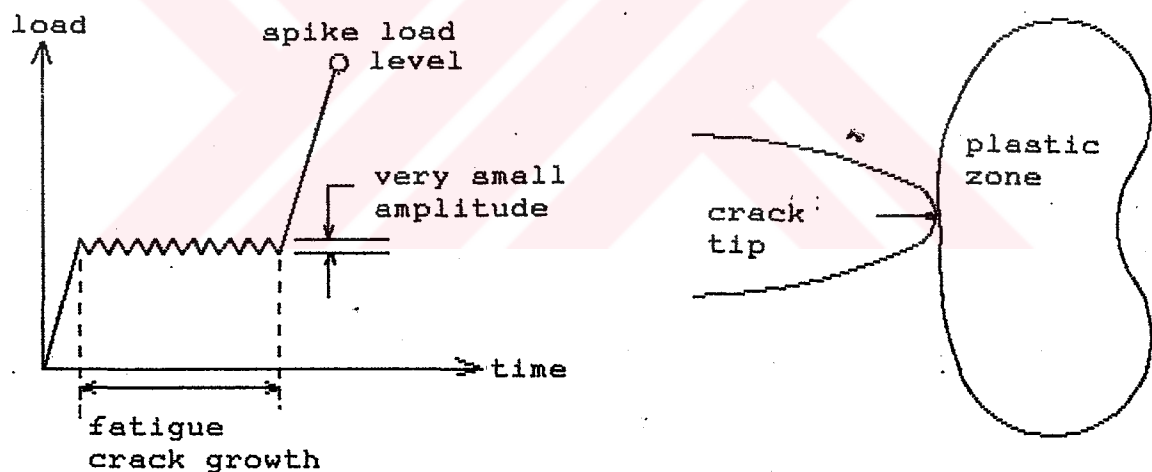
Figure 8.1: Effect of plastic deformations in front of a crack tip on the crack opening displacements. The crack i^Xxloaded to the spike load level [35].

In position B the overall stress is zero. For this reason, there will be a tension zone around the compression zone of reversed plastic flow that would be decaying away from the reversed zone balancing the compressive stresses. This tension zone causes the crack to open near the tip. Thus, after the application of the spike load the crack closure stress has
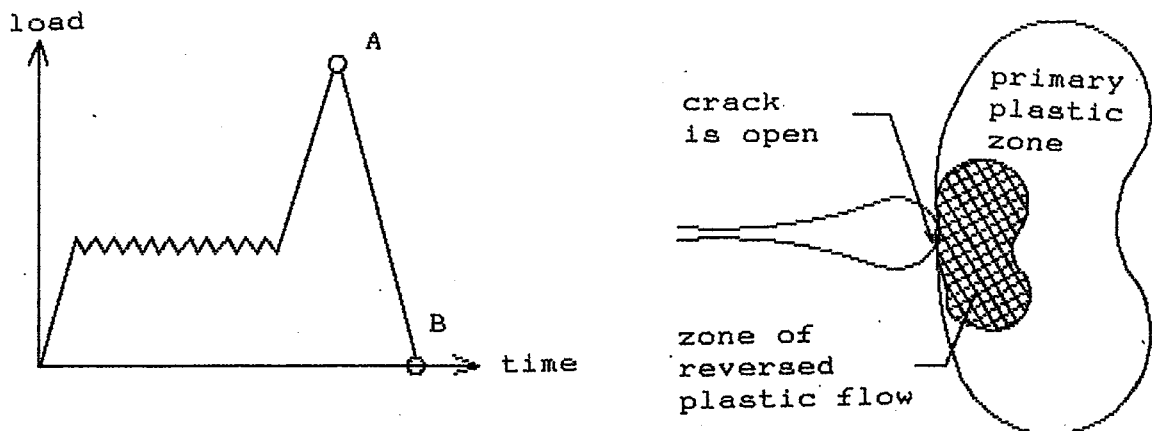
Figure 8.2: Effect of plastic deformations in front of the
crack tip on the crack tip on the crack opening
displacements. Unloading the spike load level
[35].

decreased from zero to a negative value. This may explain crack
growth acceleration after the application of an overload. In
general, it can be concluded that plastic deformations in front
of the crack tip tend to increase the crack opening
displacements. A reduction of the crack opening stress occurs.

Secondly, the effect of plastic deformations left in the
wake of a growing crack will be considered. Assuming that after
the application of the overload-underload combination, the
fictitious low-amplitude fatigue test is continued at a mean
stress (Figure 8.3). After the crack grows over a distance
equal to the primary plastic zone size, D^n the crack tip is
situated at the boundary of this zone, any further continuation
of the test will cause the crack tip to enter into the virgin
material again.

At this stage, the plastic deformations associated with
the spike load have become visible in the form of a hump
located at a distance d^n from the centre of the crack .The
width of the hump corresponds to the primary plastic zone size,
D^n . Moreover, due to the unloading of the spike load, reversed
plastic flow has caused a reduction of the hump and the area
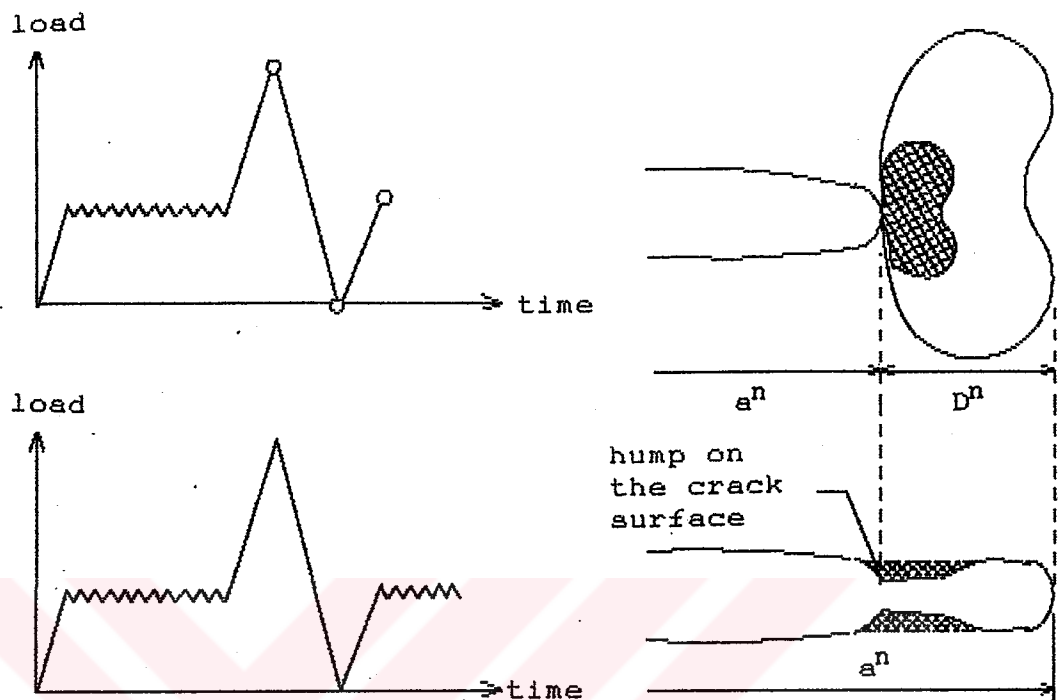
Figure 8.3: Loading sequence used analyze the behaviour of
the hump opening stress and the crack tip
situation after the application of a spike load-
underload combination [35].

affected is the same order of magnitude as the zone of reversed
plastic flow. It is seen that the presence of the hump has
locally decreased the crack opening displacements (COD).
Clearly, plastic deformations left in the wake of a growing
fatigue crack tend to increase the crack opening load. Thus,
the crack opening level will be a result of competition between
two plasticity effects.

8.4 Crack Opening Model

8.4.1 Model for a Description of Hump Opening Behaviour

The CORPUS model is basically associated with plastic
deformation left in the wake of the crack (Elber Mechanism). It
is assumed that each cycle will leave its own plastic

deformation, including its reversed plastic deformation during the unloading. Therefore the crack is covered with humps, where each hump is associated with a previous cycle.

In the model, hump opening behaviour, as shown in Figure 8.4, is approximated using a delay switch. The switch is set on after the application of a spike load and set off if the crack has grown through the spike load plastic zone. If cycle i
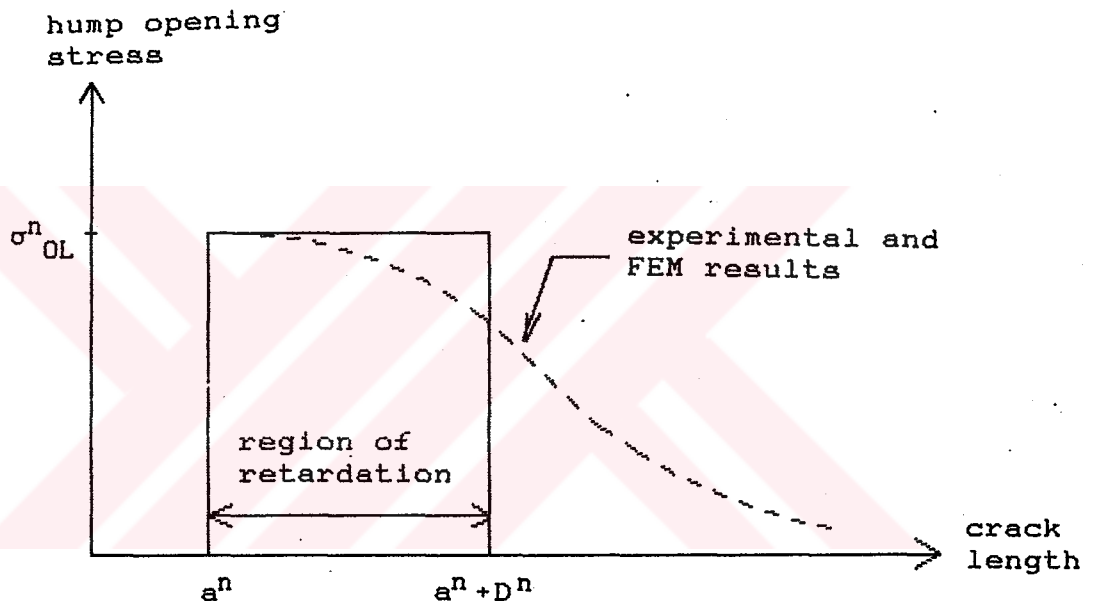
Figure 8.4: Illustration of the hump opening behaviour as observed experimentally and by the finite element method. The behaviour assumed in the madel is indicated also [35].

creates a hump, it is assumed that σ^i_{op} depends on the load σ^i_{max} applied to create the hump and on the subsequent minimum stress σ^{i+1}_{min} experienced by that hump, that is

$$S^i_{op} = g(\sigma^i_{max}, \sigma^{i+1}_{min}) \qquad if \quad a^i < a < a^i + D^i \qquad (8.8)$$

$$S_{op}^i - 0 \qquad \textit{if} \; \mathbf{a} > \mathbf{a}^{i} + D^{i} \qquad (8.9)$$

where the function g in principle will be different for different materials. Based on empirical evidence the function was defined as,

If R > 0,

$$g(\sigma_{max}^i, \sigma_{min}^{i+1}) - \sigma_{max}^i(-0.4R^4 + 0.9R^3 - 0.15R^2 + 0.2r + 0.45) \quad (8.10)$$

If -0.5 < R < 0,

$$g(\sigma_{max}^i, \sigma_{min}^{i+1}) - \sigma_{max}^i (0.1R^2 + 0.2R + 0.45) \quad (8.11)$$

where, R is the stress ratio.

$$R = \frac{\sigma^i {}_{min}^1}{\sigma^i {}_{max}} \qquad (8.12)$$

The same function is applicable to both 2024-T3 and 7075-T6 materials (Figure 5).

Newman [164] has demonstrated that the crack opening stress level does not only depend on $\sigma^i{}_{max}$ and $\sigma^i{}_{min}$ but also on the maximum stress in relation to the yield stress, i.e. on σ_{max}/σ_{YS} . de Koning defined a correction function h which adjusts the hump opening function to Newman's results. The correction function h is,

$$h - 1 - 0.2(1 - R^i)^3 \left(\frac{\sigma_{max}^i}{1.15\sigma_{YS}}\right)^3 \qquad (8.13)$$
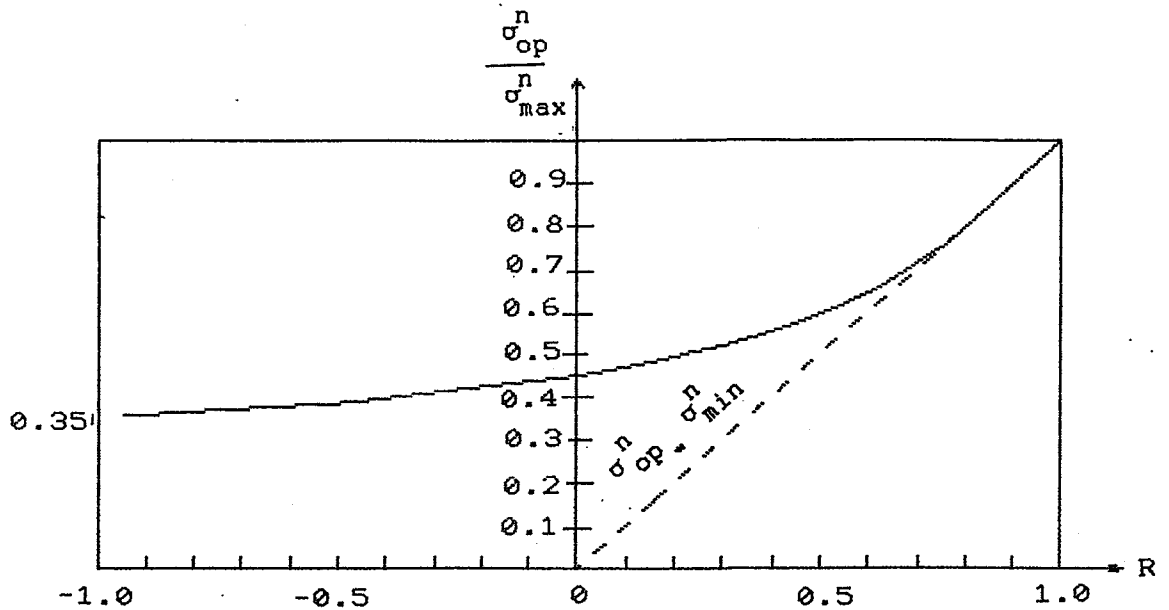
Figure 8.5: Hump opening stress plotted in relation to the stress ratio.

The corrected crack opening level is

$$S_{op}^i - g(\sigma_{max}^i, \sigma_{min}^{i+1}) \; h \qquad (8.14)$$

de Koning has applied the correction function only to 2024-T3 material.

With regard to the functional behaviour of σ_{op}^i the following observations can be made:

a. The lower the σ_{min}^i ,the flatter the hump will be; consequently it will open at a lower stress, so that σ_{op}^i decreases with σ_{min}^i .

b. Both the size of the hump and the opening stress increases with the opening stress level σ_{max}^i .

8.4.2 Effect of Application of Underloads on the Hump Opening Stress

Application of a more severe underload causes a further flattening at the hump and thus the hump opening stress decreases. This effect is illustrated in Figure 8.6. According

to the above equation, after the application of σ^n_{min} the new value of σ^i_{op} will be,

$$S^i_{op} - g(\sigma^i_{max}, \sigma^n_{min}) . h^n \qquad (8.15)$$

8.4.3 Definition of the Crack Opening Stress

Variable amplitude loading can be considered as a sequence of overload and underload combination. Application of the model implies that one delay switch per load level is introduced. Each switch accounts for the opening behaviour of one set of humps created by the application of that particular load level.
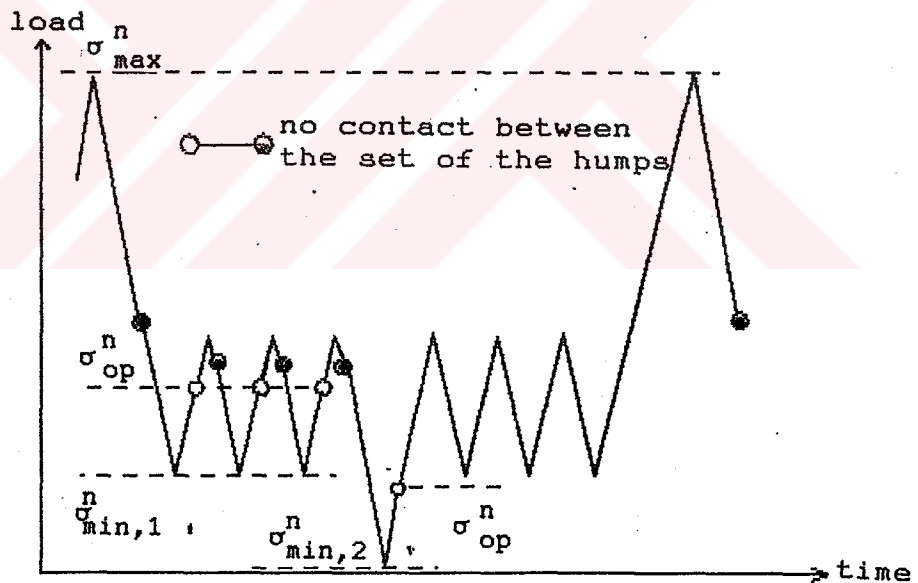
Figure 8.6: The hump created at σ^n_{max} is flattened by the application of $\sigma^n_{min,1}$ and later on, flattened by $\sigma^n_{min,2}$ [35].

The crack is assumed to be closed as long as one or more of the humps is in contact with its counterpart on the opposite surface. The hump that has last lost contact determines the crack opening stress, that is,

$$\sigma_{op} - \max(S^i_{op} . h^i) \qquad (8.16)$$

Figure 8.7 gives an illustration of crack opening stress.
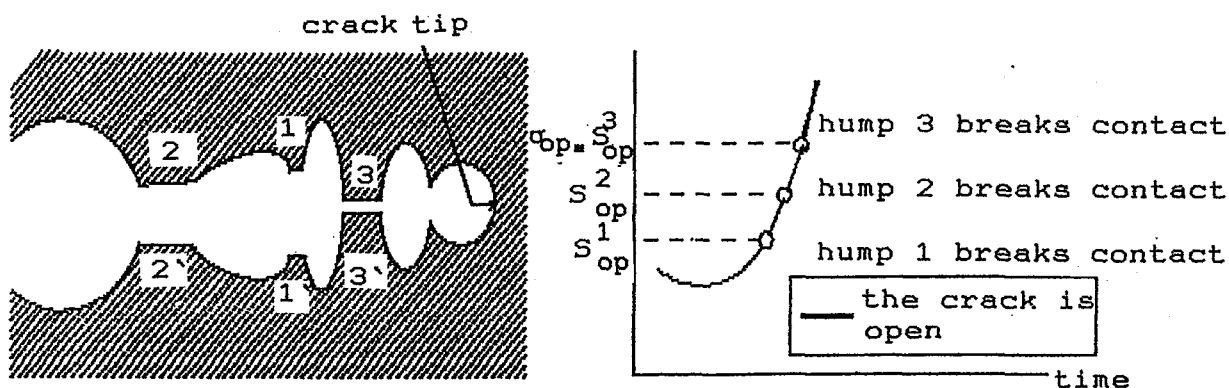
Figure 8.7: Opening behaviour of a crack tip in the case of three significant humps on the crack surface [35].

8.4.4 "Limited Memory" Properties of the Model

Using the load sequence presented in Figure 8.8 some properties are discussed hereafter. It can be seen that the first hump is created by σ^1_{max} and subsequently flattened by σ^2_{min}. The opening stress S^1_{op} of this hump is given by eq.14. It follows that

$$S^1_{op} = g(\sigma^1_{max}, \sigma^2_{min}) . h \qquad (8.17)$$

Then effective stress range $\Delta\sigma_{eff}$ for the next cycle will be

$$\Delta\sigma^1_{eff} = \sigma^2_{max} - S^1_{op} \qquad (8.18)$$
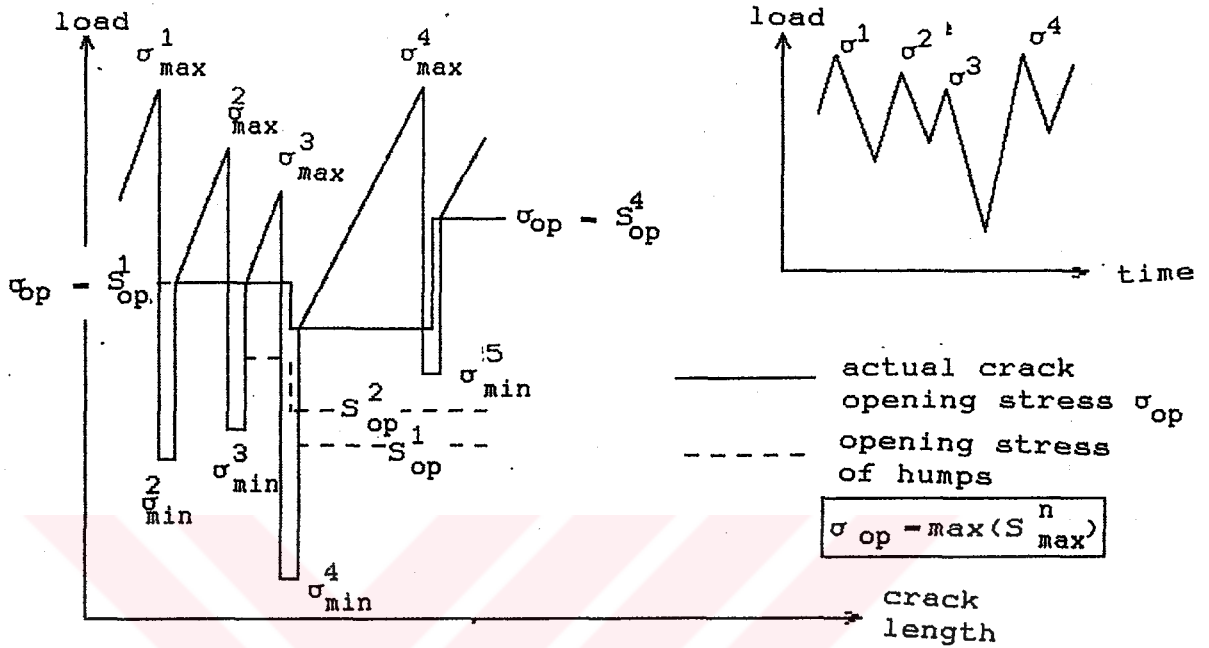
Figure 8.8: Examples of hump and crack opening behaviour [35].

The second hump is created by application of σ^2_{max}. This hump has not experienced σ^2_{min}, but in the next cycle is flattened by σ^3_{min}. Thus,

$$S^2_{op} = g(\sigma^2_{max}, \sigma^3) . h \qquad (8.19)$$

The first hump has experienced a minimum stress σ^2_{min}. Application of σ^3_{min} will not produce a further reduction of the hump provided that $\sigma^3_{min} > \sigma^2_{min}$. Therefore S^1_{op} will be the same in the second cycle. Since S^1_{op} is greater than S^2_{op}, crack opening stress will be S^1_{op} and effective stress, in the second cycle,

$$\Delta\sigma^2_{eff} = \sigma^3_{max} - \sigma_{op} = \sigma^3_{max} - S^1_{op} \qquad (8.20)$$

A third hump is produced by the application of σ^3_{max}. The subsequent negative load increment σ^4_{min} flattens all three humps, because $\sigma^4_{min} < \sigma^2_{min}$ and $\sigma^4_{min} < \sigma^3_{min}$. The hump opening stresses for the next positive load increment σ^4_{max} are respectively,

$$S^1_{op} - g(\sigma^1_{max}, \sigma^4_{min}) \cdot h \qquad (update\ S^1_{op}) \qquad (8.21)$$

$$S^2_{op} - g(\sigma^2_{max}, \sigma^4_{min}) \cdot h \qquad (Update\ S^2_{op}) \qquad (8.22)$$

$$S^3_{op} - g(\sigma^3_{max}, \sigma^4_{min}) \cdot h \qquad (8.23)$$

Since S^1_{op} still has the highest value, $\sigma_{op} = S^1_{op}$. Suppose in the next cycle σ^4_{max} is greater than all maximum loads σ^1_{max}, σ^2_{max} σ^3_{max} applied previously. Then, the hump created by the application of σ^4_{max} will dominate all of them. In the first place $\sigma^5_{min} > \sigma^4_{min}$ gives $S^4_{op} > S^1_{op}$ and, according to eq. 8.16 hump 4 becomes dominant. On the other hand, if $\sigma^2_{min} < \sigma^5_{min}$ then humps 1,2,3 will experience a minimum load more severe than the previous σ^4_{min}. For the updated values of hump opening stresses, it follows that $S^4_{op} > S^1_{op} > S^2_{op} > S^3_{op}$. It is seen that after the application of any negative load increment, hump 4 governs the crack opening behaviour. In general, it can be concluded that the effect of previous hump, j, on the crack opening behaviour is overruled by the application of a more severe maximum load σ^i_{max}, that is, $\sigma^i_{max} > \sigma^j_{max}$. In this way, application of a relatively high load level erases part of the memory. Besides, the effect of hump j is also erased permanently if $a > a^j + D^j$, namely, when the crack passes through the plastic zone created by σ^j_{max}.

8.5 Retardation Regions

The plastic zone size depends on the state of stress at

the crack tip, plane stress, plane strain or a transition between those two conditions. A characteristic feature of the CORPUS model is that it also distinguishes between a plastic zone extending into virgin (elastic) material and a plastic zone induced in material that was already plastically deformed before. These two types are respectively called primary and secondary plastic zones. de Koning derived a special equation for the primary plastic zone. This equation was based on the Irwin type equation. Due to his obversation that Irwin's equation underestimates the plastic zone at load levels approaching the yield limit, he introduced some corrections to account for this fact. It is formulated as

$$\frac{D}{a} = \frac{1-\alpha\left(\frac{\sigma_{max}}{\sigma_{YS}}\right)^2 + \left(\frac{a}{b}\right)^2 - \sqrt{\left[1-\alpha\left(\frac{\sigma_{max}}{\sigma_{YS}}\right)^2 + \left(\frac{a}{b}\right)^2\right]^2 - 4\left(\frac{a}{b}\right)^2}}{2\left(\frac{a}{b}\right)^2} - 1$$

(8.24)

where b is the semi width of the specimen and α depends on the state of stress. For plane stress $\alpha = 1/1.32$ and for plane strain $\alpha = 1/9$. For 7075-T6 material with a high yield stress, the plastic zone size equation is obtained by simplifying eq.24.

$$D = a\,\alpha\left(\frac{\sigma_{max}}{\sigma_{YS}}\right)^2\left[1 + \left(\frac{a}{b}\right)^2 + \alpha\left(\frac{\sigma_{max}}{\sigma_{YS}}\right)^2\right]$$

(8.25)

In the CORPUS model, the crack tip state of stress depends on the size of the plastic zone relative to the thickness. First, the plastic zone size is calculated under plane stress condition (D_{ss}). If $D_{ss} > 0.5t$ then the plastic zone size is assumed to be in plane stress. If $D_{ss} < 0.35t$, the plastic zone is assumed to be in plane strain. The plane strain size is denoted by D_{sn}. During the transition from plane strain to plane stress, ($0.35t < D_{ss} < 0.5t$), the plastic zone

size is

$$D = D_{nn} + 2D_{sn} [\frac{(\frac{D_{sn}}{t} - 0.35)}{0.15}]^4 \frac{(D_{sn} - D_{nn})}{t} \qquad (8.26)$$

A plot of the relation between the delay region and the plane stress plastic zone size is given in Figure 8.9.
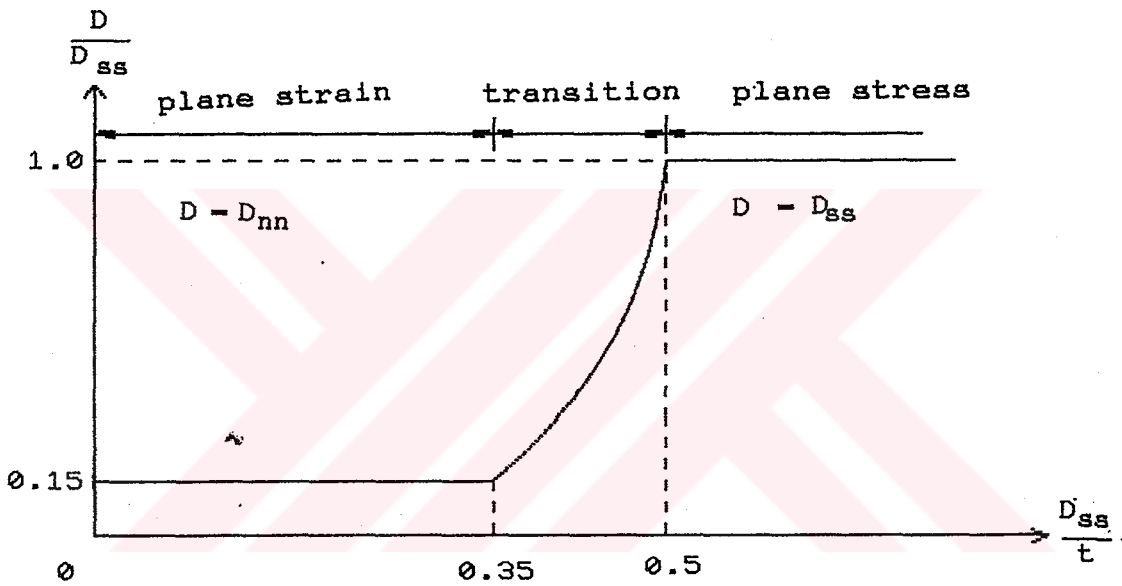
Figure 8.9: The delay region plotted in relation to the plane stress plastic zone size [10].

Secondary plastic zones are always assumed to develop under plane strain condition. The size of a secondary plastic zone is,

$$D = \frac{1}{9\pi} (\frac{\Delta K_{eff}}{2\sigma_{ys}})^2 \qquad (8.27)$$

This equation is based on the Irwin plastic zone size approximation with $\alpha = 1/9$ for plane strain and $2\sigma_{YS}$ instead of σ_{YS} in view of reversed plastic deformation present in the primary plastic zone.

8.6 Modelling of the Material Memory

During crack growth under variable amplitude loading, various primary and secondary plastic zones will be created. If they can affect σ_{op} in later cycles, they must be stored in the material memory. In Figure 8.10 a schematic picture is given with two primary zones and two secondary zones. The primary plastic zone (PPZ) was formed at $a = a_2$. It became a PPZ because it penetrated elastic material, which means,

$$a_2 + dp_2 > a_1 + dp_1 \tag{8.28}$$
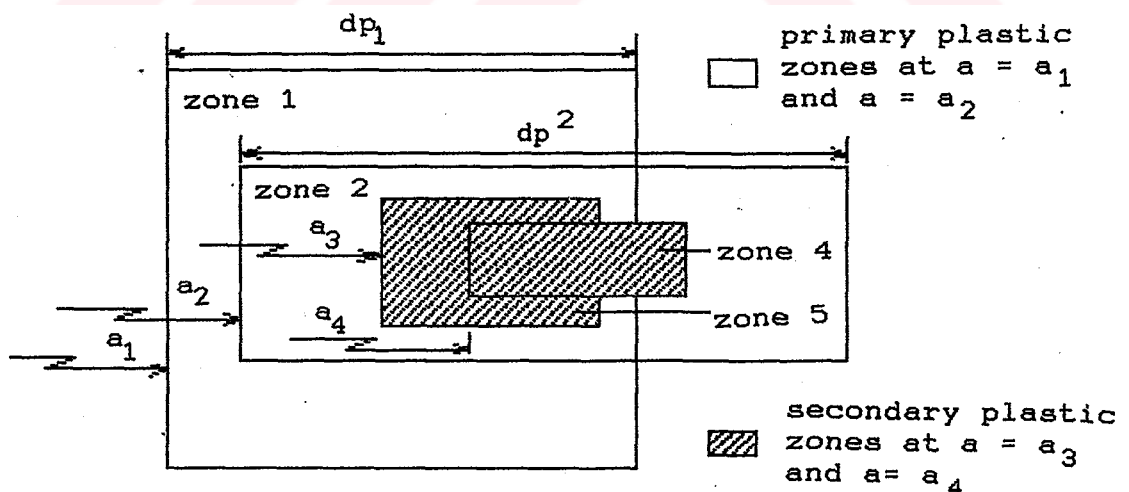
Figure 8.10: Overlapping plastic zones in the CORPUS model [7].

At $a = a_3$ a primary plastic zone was not formed because

its size dp_3 , calculated using eq. 8.24, was not large enough to penetrate elastic material. In other words,

$$a_3 + dp_3 < a_2 + dp_2 \qquad (8.29)$$

The load cycle occurring at a = a_3 thus created a secondary plastic zone with a size according to equation 8.27.

Fortunately not all plastic zones can affect σ_{op}, because their effect on σ_{op} is overruled by other plastic zones, or the delay switch was turned off. As a consequence, only a limited number of plastic zones must be stored in the material memory.

If the crack is growing, it will reach a size a = a_1 + dp_1. At that moment the delay switch is turned off and the first PPZ can be removed from the memory.

The second PPZ was formed at a = a_2. If σ^2_{max} exceeds σ^1_{max} it will create a larger hump and the hump of the first PPZ can never become dominant afterwards. The first PPZ can thus be erased from the material memory.

From the above arguments it follows that the σ_{max} values associated with primary zones that should be stored in memory must form a series of decreasing values. These values, named history values are labelled as σH_{max} values. In a similar way, the arguments on creating and reducing humps by downward loads, imply that there is one σ_{min} value associated with each PPZ, and secondly the σH_{min} values must form a series of increasing, or at least equal values which can not occur in the PREFFAS model. Each pair of σH_{max} and σH_{min} of a plastic zone is connected with an S_{op} value, but the SH_{op} values of successive plastic zones do not necessarily form an increasing or decreasing series of values in contrast to the PREFFAS model. For a crack tip located in overlapping plastic zones, the S_{op} values of the zones have to be checked to find the maximum value. In addition to σH_{max}, σH_{min}, SH_{op} the plastic zone size and its location (a,D) must also be stored in the material

memory.

If a PPZ is not formed, and the crack is still opened, a secondary plastic zone (SPZ) is formed. This may occur in many cycles. However, only the historic SPZ's have to be stored in the memory. A SPZ is a historic SPZ if it can have an effect on σ_{op} in subsequent cycles. The hump and delay switch concept are also applicable to the historic SPZ's. This implies that again the σH_{max} and the σH_{min} values form a decreasing and increasing or equal series of stress levels respectively, whereas again no specific sequence applies to the associated SH_{op} values. Moreover, in view of the hump concept the combined series of σH_{max} and σH_{min} values of both PPZ's and SPZ's together must form such series as schematically shown in Figure 8.11. With respect to σH_{op} of the SPZ's there is a limitation. If in Figure 8.10 σH_{op} of zone 3 is lower than the σH_{op} levels of the σH_{op} level of the two PPZ's (zone 1 and 2), there is no need to store σH levels of zone 3 in memory. SPZ's by definition are embedded PPZ's. If these PPZ's have higher σH_{op} than SPZ, the hump of the secondary plastic zone will always remain less significant than the humps of the PPZ's. The delay switch of the SPZ's will always be turned off before PPZ's. In other words, the σH_{op} values of the SPZ's must all be higher than the lowest σH_{op} of the PPZ's.

The above characteristic features are the logical result of the hump and the delay switch concepts. Some consequences are recapitulated below:

a. A PPZ is formed only if plastic deformation enters the elastic material. More than one PPZ can exist at the same time.

b. SPZ's must be stored in the material memory when they can have effect on σ_{op} in subsequent cycles. The number of such historical SPZ's will be limited because they are easily erased either by high σ_{max} peaks, low σ_{min} peaks or by turning

off the delay switch as a result of crack growth.

Several examples of erasing plastic zones, of decreasing σH_{min} and σH_{op} are schematically illustrated in Figure 8.11.

σ_{max} erases PPZ No. 2 nd 3

σ_{max} erases SPZ No. 4, 5, 6 and introduces a new PPZ or a new SPZ

σ_{min} resets history levels of SPZ No. 5 and 6 ($\sigma H_{min,5}$ = $\sigma H_{min,6}$ = σ_{min}) $\sigma H_{op,5}$ and $\sigma H_{op,6}$ is reduced

σ_{min} resets history levels of PPZ No. 2 and 3 $\sigma H_{min,2}$ and $\sigma H_{min,3}$ are equal to σ_{min} All SPZ'are erased
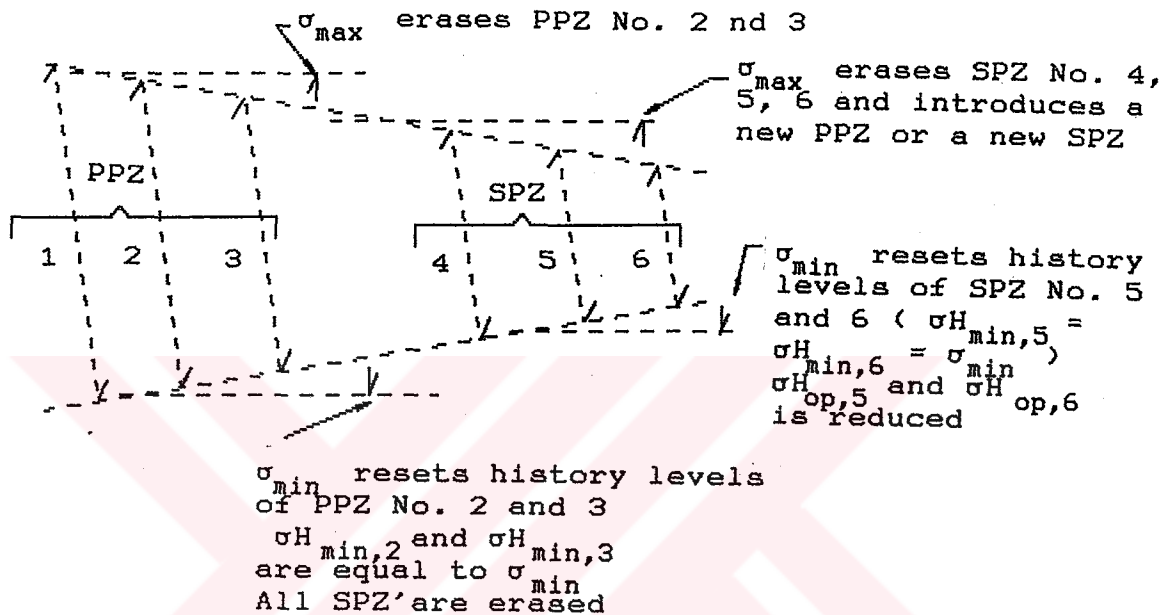
Figure 8.11: Series of decreasing σH_{max} and increasing σH_{min} values inthe COPUS model. Consequunces of some σ_{max} and σ_{min} values if they occur [7]

8.7 Interaction of overloads

The model described in the previous sections was developed specifically for the evaluation of crack opening stress levels resulting from application of single overload-underload combinations. In the previous version of the model, de Koning applied the model to 7075-T6 material and obtained satisfactory results. However, application of the model to 2024-T3 material with lower yield strength and higher ductility resulted in highly conservative predictions. This was due to

the interaction of overloads which played an important role in 2024-T3 material unlike 7075-T6 material. He also carried out an experiment with constant amplitude load sequence interrupted twice for the application of overload-underload combination. He observed that upon unloading the second overload, the load bearing capacity of the relatively larger hump (associated with the first overload-underload combination) reduces reversed plastic flow in the actual plastic zone. Thus, interaction between the overloads leads to a higher hump and, therefore the hump opening stress level of the second overload is higher than in the case of a hump created by application of a single overload.

In the case of a single overload-underload combination the hump opening stress is given by eq.14. If there is interaction with another overload-underload combination, then the hump opening stress is higher than S_{op} according to eq.14 ,that is

$$S_{op}^n \geq g(S_{max}^n, S_{min}^n) \qquad (8.30)$$

With regard to the application of a series of overloads, each being of the same magnitude, it will be assumed that the value of S_{op} possesses a certain upperbound. This bound is considered as the stationary value of S_{op} for the case of multiple overloads. To define the stationary level a parameter m_{st}^n ($0 \leq m_{st}^n \leq 1$) is introduced. Using this parameter, the range of valid S_{op} values is bounded by the following assumption

$$\underbrace{g(\sigma_{max}^n, \sigma_{min}^n)}_{\substack{\text{lower bound} \\ \text{single overload}}} \leq \sigma_{op}^n \leq \underbrace{g(\sigma_{max}^n, \sigma_{min}^n) + m_{st}^n[\sigma_{max}^n - g(\sigma_{max}^n, \sigma_{min}^n)]}_{\substack{\text{upper bound} \\ \text{stationary } s_{op}^n}}$$

$$(8.31)$$

For the 2024-T3 material under consideration, he observed that the stationary value of S_{op} depends on the proportion between the amount of crack growth occurred during low amplitude loading in the interval between the application of overloads and the overload plastic zone size. For the case of overload plane stress plastic zones this behaviour is approximated by,

$$m_{st}^n = 0.1+0.2\frac{\Delta a}{D^n} \qquad if \quad 0 < \frac{\Delta a}{D^n} \leq 0.25 \qquad (17)$$

$$m_{st}^n = 0.15 \qquad if \quad 0.25 < \frac{\Delta a}{D^n} \leq 1 \qquad (8.32)$$

$$m_{st}^n = 0 \qquad if \quad \frac{\Delta a}{D^n} > 1$$

where Δa is the amount of crack growth in the interval between the application of overloads and, D^n, stands for the plastic zone size of the overload. A graphical representation of m_{st}^n is given in Figure 8.12. It is noted that, in the region corresponding to $0.25 < \Delta a/D^n \leq 1$, the stationary value, m_{st}^n, is seldom reached due to the finite width of the specimen. de Koning extrapolated the values presented for this region. In the regime corresponding to $\Delta a/D^n > 1$, the overload interaction is ignored. The overloads are then treated as single overloads.

m_{st}

0.2

0.1

0   0.25   1 $\dfrac{\Delta a}{D}$
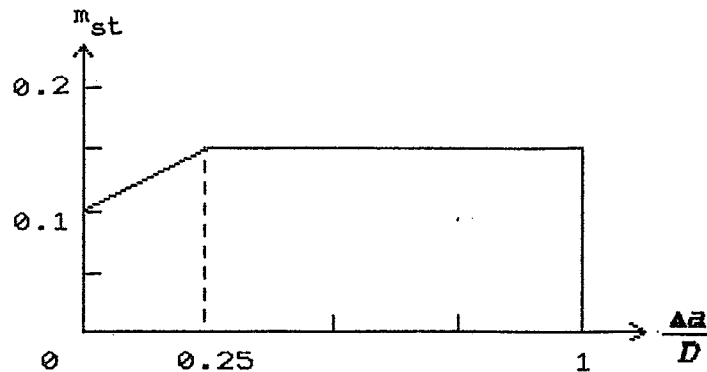
Figure 8.12: The stationary parameter
of overload interaction

8.7.1 Constant Amplitude Case

Under constant amplitude loading the plastic zone will extend in each cycle into elastic material. This implies that each cycle is an overload for the previous cycle. In this case multiple interaction will occur, which will raise S_{op} For the constant amplitude case, Δa is small compared to D^n. Therefore, $\Delta a/D^n$ value can be taken as zero. It then follows from eq.32 that $m^n_{st} = 0.1$.

$$S^n_{op} - g(S^n_{max}, S^n_{min}) + 0.1[S^n_{max} - g(S^n_{max}, S^n_{min})] \qquad (8.33)$$

8.7.2 Variable Amplitude Case

In general, a large number of overloads are required to reach the stationary condition of S_{op}. The S_{op} is relaxed to the stationary value in a stepwise manner starting with the single overload value. To describe relaxation process a parameter was introduced. This parameter should be updated whenever a new overload is applied.

$$S^n_{op} - g(S^n_{max}, S^n_{min}) + m^n[S^n_{max} - g(S^n_{max}, S^n_{min})] \qquad (8.34)$$

For $m^n = 0$, S^n_{op} is equal to $g(S^n_{max}, S^n_{min})$ for the single overload underload case, and for $m^n = m^n_{st}$ the S^n_{op} is equal to the stationary level. The updating equation of m^n is,

$$m^n_{new} = m^n_{old} + \delta \left[m^n_{st} - m^n_{old} \right] \frac{\Delta a}{D^d} \qquad (8.35)$$

where δ is the relaxation factor, Δa is the crack extension between the overloads, and D^d is the plastic zone size of the dominant hump of preceding overloads which has the highest crack opening level selected from the primary plastic zones. For the 2024-T3 material the value δ has been chosen to be 0.28. It should be noted that the upperbound, m^n_{st}, itself also depends on the $\Delta a/D^n$ value. Therefore, its values must be updated at the same time.

The stationary condition was first considered for interaction effects of overloads with the same load level in the plane stress condition. In a more general load sequence, interaction of overloads with different load levels and plastic zones under different conditions must be considered. de Koning introduced two corrections on the relaxation factor, δ, to account for the effects mentioned above, that is

$$\delta = 0.28 \, \delta_1 \, \delta_2 \qquad (8.36)$$

where 0.28 is the relaxation factor adopted for the 2024-T3 material. δ_1 accounts for the differences in overload levels and δ_2 accounts for the effect of reduced overload interaction plane strain. These corrections are given by,

$$\delta_1 = \left[\frac{4 \, D^d \, D^n}{(D^d + D^n)^2} \right]^4 \qquad if \ D^n \leq D^d \qquad (8.37)$$

$$\delta_2 - \frac{D^d}{D^n} \qquad\qquad if \ \ D^n \succ D^d \qquad (8.38)$$

and,

$$\delta_2 - \frac{D^d}{D^n_{ss}} \qquad\qquad 0 \leq \delta_2 \leq 1 \qquad (8.39)$$

where D^d is the plastic zone size associated with the dominant hump, which provides the highest crack opening level. D^d and D^d_{ss} are respectively the actual plastic zone size and its value for the hypothetical case of plane stress with $\alpha = 1/1.32$ for the dominant hump. D^n is the current plastic zone size. m^n_{st} is determined according to eq.32 by using D^d instead of D^n. δ_1 is plotted in Figure 8.13. The graph shows that the interaction is smaller if D^n and D^d are significantly different, whereas the interaction is larger if the two sizes are about the same. It should be indicated that m^n_{old} in eq.35 is the value corresponding to D^d not necessarily the value immediately preceding m^n_{new} and that in eq.35 for the value of m^n_{old} the value of m^d_{old} is substituted if $\delta_1 \delta_2 m^d_{old} > m^n_{old}$.

Interaction of multiple overloads are applied only for peak loads which produce a primary plastic zone.

de Koning did not apply the interaction of overloads for 7075-T6 material, since no improvement in the predictions were observed.

8.8 Failure Analysis

In an application of the crack growth model to a practical problem, the computations must end when the final failure occurs. For this purpose de Koning has chosen two criteria; net section yield and fracture of the specimen. The condition for net section yield was formulated as,

where b is the half width of the specimen
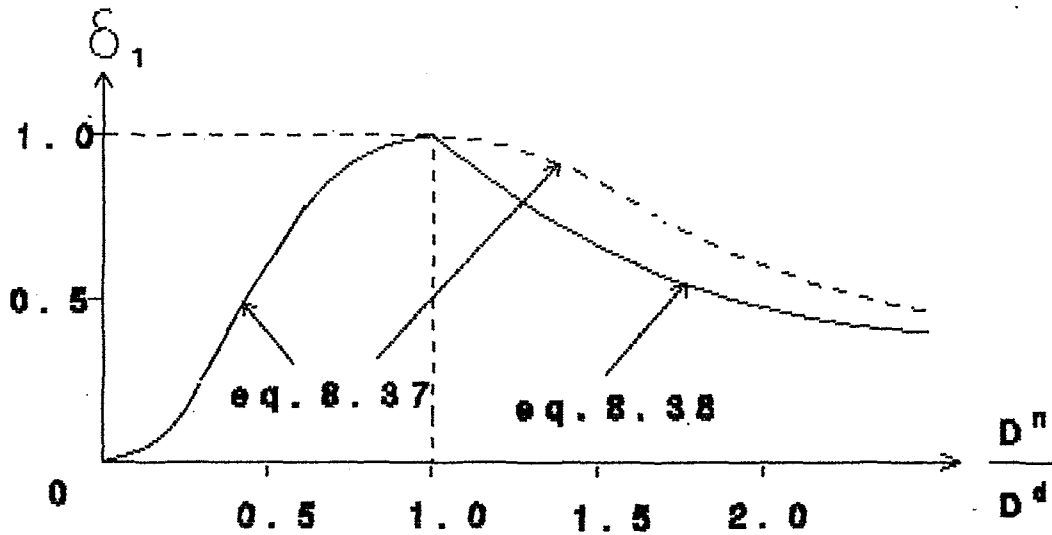
Figure 8.13; The correction factor, δ_1 , for the relaxation factor, δ, accounting for the effects of different load levels.

$$\textit{Net Section Yield} \qquad \textit{if} \quad \sigma_{max}^i \geq \sigma_{YS}(1-\frac{a^i}{b}) \qquad (8.40)$$

The test on fracture is,

$$\textit{Fracture} \qquad \textit{if} \quad K - Y\,\sigma_{max}\sqrt{\pi a^i} \geq K_{IC}$$

where K_{IC} is the fracture toughness of the material.

8.9 Prediction Results

de Koning has provided material parameters for 2024-T3 Alclad and 7075-T6 Clad materials to run the CORPUS model, also Padmadinata [7] has also determined material parameters for 2024-T3 bare material.

The parameters used in present calculations are given below.

a. 2 mm 2024-T3 Alclad material

$$\sigma_{YS} = 360 \text{ MPa}$$
$$K_{IC} = 65 \text{ MPa m}^{\frac{1}{2}}$$
$$C = 1.26 * 10^{-10}$$
$$n = 3.7$$
$$\delta = 0.28 \, \delta_1 \, \delta_2$$

b. 2 mm 7075-T6 Clad material

$$\sigma_{YS} = 500 \text{ MPa}$$
$$K_{IC} = 70 \text{ MPa m}^{\frac{1}{2}}$$
$$C = 1.6 * 10^{-9}$$
$$n = 2.5$$
$$\delta = 0$$

c. 2 mm 2024-T3 Alclad material

$$\sigma_{YS} = 394 \text{ MPa}$$
$$C = 2.9443 * 10^{-11}$$
$$n = 4.1$$
$$\delta = 0.28 \, \delta_1 \, \delta_2$$

de Koning has applied the model to F-27 and F-4 spectra. Later, Padmadinata has applied it to F-27, F-4 miniTwist, Twist, FALSTAFF, CN 235 spectra and to some variable amplitude tests (Misawa/Schijve tests). de Koning has made some minor modifications in eq.'s 11 and 13 that Padmadinata has adopted in his thesis. For this reason there exist some differences between the two. In the present thesis, the computer program was run for the F-27, F-4, TWIST and miniTWIST spectra and the Misawa/Schijve tests. Descriptions of the flight simulation spectra have been given in chapter 1.

A presentation of the tests and prediction results are given below.

F-27 and F-4 Spectra

The F-27 and F-4 load spectra were described in chapter I. In the F-27 flight simulation tests, the width and thickness of the center cracked specimens were 160mm and 2mm respectively, with a center notch width, $2a_0$, of 7 mm [7]. This load is referred to as case NN (normal gust spectrum, normal ground stress level). Variables studied were the gust spectrum severity, the ground stress (σ_{gr}) severity and the mean stress in flight (σ_{mf}). A severe and a light gust spectrum were obtained by increasing the σ_a / σ_{mf} values of the normal gust spectrum (table 8.2). Several ground load severities were used with σ_{gr}/σ_{mf} varying from -0.5 (severe), +0.125 (light). Table 8.1 gives a description of load variables.

flight type code	relative gust amplitude σ_a/σ_{mf}		
	basic-program	severe gust	light gust
10	1.25	1.39	1.11
9	1.15	1.28	1.02
8	1.05	1.18	0.92
7	0.95	1.08	0.82
6	0.85	0.97	0.73
5	0.75	0.87	0.63
4	0.65	0.76	0.54
3	0.55	0.65	0.45
2	0.425	0.515	0.335
1	0.30	0.39	0.21

Table 8.1: The gust amplitude for the basic programme and the derived severe gust and light gust versions. F-27 spectrum [7].

		σ_{gr}/σ_{af}		gust severity		
		2024-T3	7071-T6	light	normal	severe
ground stress severity	light*	+0.125	+0.125	LL	NL	SL
	light		-0.125	LL*	NLw*	SL*
	normal	-0.234	-2.54	LN	NN	SN
	severe	-0.5	-0.5	LS	NS	SS
				gust		

(*) Applied to 7075-T6 only

Table 8.2: Letter codes of the gust spectrum and ground load
severities, based on the F-27 spectrum [7].

Material: 7075-T6 Clad

(a)   3.5mm ⇢35mm

N (flights)

spectrum variant	σ_{MF} (MPa)	test	predictions	prediction/ test
NN	90	7000	8500	1.2
	80	10700	11200	1.0
	70	16500	15100	0.9
LL*		27700	25900	0.9
LN	70	25300	23900	0.9
LS		21400	22100	1.0
NL		24600	17500	0.7
NL*	70	17000	16200	1.0
NN		16500	15100	0.9
NS		12400	13200	1.1
SL		17500	12500	0.7
SL*	70	11800	11300	1.0
SN		9700	10700	1.1
SS		8734	9600	1.1
F-4	63.7	10600	13400	1.3

N = normal, S = severe, L = light, L* = not so light

First capital refers to gust spectrum, second one to ground
stress σ_{gr}.

Table 8.3: Crack growth lives, tests and prediction results for
F-27 and F-4 spectra (7075-T6 Clad material).

Material: 2024-T3 Alclad

(a) 3.5mm →25mm

N (flights)

spectrum variant	σ_{MF} (MPa)	test	predictions	prediction/ test
NN	110 90 70	10900 36300 123000	7800 39400 107100	0.7 1.1 0.9
LL LN LS	100	72800 31200 19000	45100 32800 19000	0.6 1.1 1.1
NL NN NS	100	44000 18250 10250	18700 18300 8700	0.4 1.0 0.8
SL SN SS	100	23500 11500 5400	7700 7300 5400	0.3 0.6 1.0
F-4	91	6300	6800	1.1

N = normal, S = severe, L = light

First capital refers to gust spectrum, second one to ground stress σ_{gr}.

Table 8.4: Crack growth lives, tests and prediction results for F-27 and F-4 spectra (2024-T3 Alclad material).

TWIST Spectrum

The tests were carried out on central cracked specimens (width W = 100, thickness t = 2mm) of two materials, 2024-T3 Alclad and 7075-T6 Clad. The test variable was the truncation level. For 2024-T3 Alclad material, truncated load levels were II, III, IV and V, while for 7075-T6 Clac material truncation levels were I, II, III, IV and V.

a. Material: 2024-T3 Alclad

   (a) 4mm → 24mm

   N (flights)

Truncation level	test	predictions	prediction/test
II	64900	53700	0.8
III	21750	19700	0.9
IV	12600	8000	0.6
V	8400	5400	0.6

a. Material: 7075-T6 Clad

   (a) 3.5mm → 25mm

   N (flights)

Truncation level	test	predictions	prediction/test
I	4400	3300	0.7
II	4000	2800	0.9
III	3400	2500	0.7
IV	3000	2400	0.8
V	3600	2400	0.7

Table 8.5: Crack growth lives, test and prediction results for TWIST spectrum.

miniTWIST Spectrum

The tests were carried out by Padmadinata using central cracked specimens with 160 mm width and 2mm thickness. The test variable was ground load severity.

Material: 2024-T3 Alclad

(a) 6mm → 30mm

N (flights)

ground stress	test	predictions	predictions/test
$-0.5\sigma_{mf}$	13000	11100	0.8
0	28000	13700	0.5

Table 8.6: Crack growth lives , tests and prediction results for miniTWIST spectrum.

Simplified flight simulation loading tests

The tests were carried out by Misawa/Schijve using central cracked specimens with a nominal thickness 2 mm and a width of 100 mm. The results of the tests were taken from reference [7]. Three types of flight load sequence were adopted. The load sequences used in these test series are shown in Figure 8.13. Two values were adopted for the number of cycles per flight (m). These were 5 and 100. In Figure 8.14, only the first one is presented.
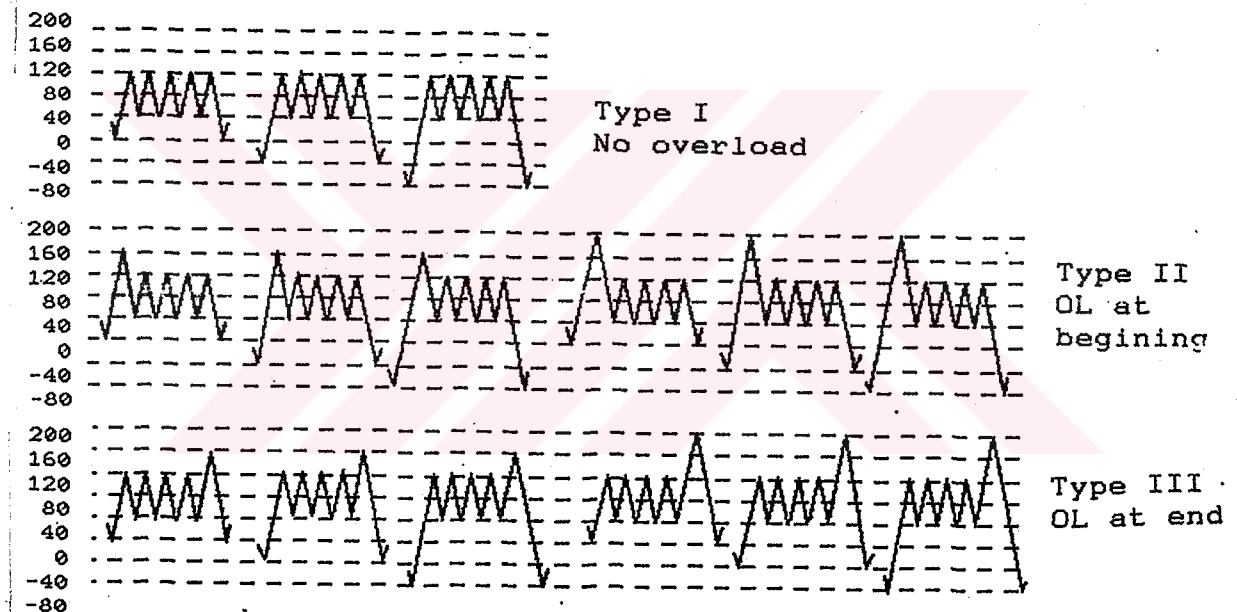
Figure 8.14: Load sequences in the flight-simulation tests with five cycles per flight [7]

Material: 2024-T3 bare

m = 5 (cycles/flight)

type	σ_{gr} (MPa)	σ_{OL} (MPa)	tests (kc)	predictions (kc)	prediction/ test
I	0		48	62	1.3
	-40		49	53	1.1
	-80		43	48	1.1
II	0	200	21	19	0.9
		160	45	48	1.1
	-40	200	17	14	0.8
		160	38	36	0.9
	-80	200	14	11	0.8
		160	31	29	0.9
III	0	200	22	19	0.9
		160	46	42	0.9
	-40	200	16	14	0.8
		160	36	28	0.8
	-80	200	15	11	0.7
		160	31	22	0.7

Table 8.7 : Crack growth lives, tests and prediction results for the Misawa/Schijve tests (m = 5)

Material: 2024-T3 bare

$m = 100$ (cycles/flight)

type	σ_{gr} (MPa)	σ_{OL} (MPa)	tests (kc)	predictions (kc)	prediction/ test
I	0		64	72	1.1
	-40		58	72	1.2
	-80		60	71	1.2
II	0	200	265	350	1.3
		160	195	284	1.5
	-40	200	213	267	1.3
		160	145	258	1.8
	-80	200	139	215	1.5
		160	133	237	1.8
III	0	200	302	281	0.9
		160	172	142	0.8
	-40	200	209	165	0.8
		160	135	84	0.6
	-80	200	131	105	0.8
		160	122	57	0.5

Table 8.8: Crack growth lives, tests and prediction results for the Misawa/Schijve tests ($m = 100$)

IX.   DISCUSSION

In   evaluation   of   crack   propagation   models,   three
criteria are important. The model should (1) accurately predict
crack growth; (2) indicate the trends of the effects of design
variables;   (3)   be   applicable   in   a   wide   range   of   crack
phenomena.   In view of this   criteria an account   of the CORPUS
model will be given.

9.1   Effect of Design Stress Level

Different design stress levels were applied in the F-27
tests   (Tables   8.3   and   8.4).   For   the   2024-T3   and   7075-T6
materials, respectively 110,   90, 70   MPa and   90, 80,   70 Mpa
mean flight stresses were used. The prediction results agree
rather well with the test results.

9.2   Effect of Gust Load Severity

The gust load severity effects were investigated in the
F-27 tests (Table 8.3 and 8.4). The Gust load severity effect
is well predicted for the 7075-T6 material. But, for the 2024-
T3 material the predictions are not good in some cases. The
ratios between predicted life and test life are 0.6, 0.4 , 0.3
for the cases LL 100 (light gust), NL 100 (normal gust) and SL
100 (severe gust), respectively.

9.3   Effect of Load Sequence

Load   sequence variations were applied in the Misawa/
Schijve tests (Table   8.7 and 8.8). The predictions of the
CORPUS model indicate a significant sequence effect in types II
and III, especially for m=100 which contradicts test results.
The tests indicate similar results for the two sequences,
whereas, CORPUS predicts systematically larger lives   for

sequence II. This was associated with a different choice of σ_{min} values for the calculation of S_{op} . In the CORPUS model preceding minimum loads have no effect on hump opening level. For the load sequence type II, where the overload cycle precedes small cycles, S_{op} is determined by the maximum stress of the overload, σ_{OL} , and the minimum stress of the small cycles. However, for the load sequence type III, where the overload cycle follows small cycles, S_{op} is determined by the maximum stress of the overload and the more severe gust load. Therefore, the crack opening stress level in load sequence type II is higher than in type III which leads to a longer life.

9.4 Effect of Ground Stress Level

The effect of ground stress levels can be observed in tests with miniTWIST and F-27 spectra, and in the Misawa / Schijve tests. Under F-27 spectrum, for 7075-T6 material the effects of variations of the ground stress level are well predicted. As for 2024-T3 material the effect of ground stress level is overestimated for light spectra; LL, NL, SL . As a result, The predictions are very conservative. Under miniTWIST, the tests were carried out for the normal ground stress (σ_{gr} = $-0.5\sigma_{mf}$) and for a light ground stress (σ_{gr} = 0) (Table 8.6). Again the predictions are good for the normal ground stress and conservative for the light ground stress. They are respectively 0.9 and 0.5. Prediction results are good for Misawa / Schijve tests, particularly for m=5.

Padmadinata has given an explanation for the poor performance of the CORPUS model in predicting the crack growths of light ground stress spectra. The Common feature of these spectra was that the most severe downward load was the most severe minimum gust load. Although it is a rarely occurring load (once in 2500 flights), it has a predominant effect on the crack opening stress level. It is due to the assumption that underloads affect hump size in its entirety. The reduced hump

opening level continues until the crack moves out of overload induced plastic zone. In contrast, in the ONERA model, because of fast relaxation of K_{mineq} , the crack opening level resumes its previous value. As a result, underloads have a limited effect on the crack opening level. In this respect, CORPUS doesn't agree with the experimental trend. Based on this reasoning, Padmadinata developed a concept of underload affected zone in his modified CORPUS model [7]. The Crack opening level is determined by the most severe maximum load and the most severe minimum load, each having their own delay switch. With this assumption, history value and secondary plastic zone concepts are eliminated. Whereas the poor predictions of the CORPUS model are improved in its new version, the compatibility of the modified model to the real crack growth mechanisms is questionable. Let us consider an overload-underload combination, the underload immediately preceding the overload. In the CORPUS model, since the hump size can only be reduced by a minimum load that occurs after hump is created, the underload would have no effect on the hump created by the overload. In the modified model, since the underload would create a dominant reversed plasticity at the crack tip, it will have full effect on the hump opening level. On the other hand, experiments give a contrary trend. If an underload immediately precedes an overload, the effect of the underload on overload induced retardation would be limited.

The approach used in the ONERA model seems more appealing. However, the function used in the model for the relaxation of K_{mineq} , is not a proper one, so that the model does not predict correctly the effects of ground stress level.

9.5 Effect of Truncation

Effect of truncation can be observed in the TWIST tests (Table.8.5). The trend is correctly predicted.

9.6 Prediction of Crack Increments

Some fractographic investigations [43] and measurements of crack increments [7] have shown that crack increments predicted by the CORPUS model were underestimated for the most severe flight. In addition, the predictions overestimate the total crack growth life and underestimate Δa of the severe flights. It must be concluded that the prediction model must overestimate crack growth in the less severe flights. This may be attributable to the involvement of other crack growth mechanisms, such as ductile tearing in high ΔK values. This aspect of crack growth was discussed in reference [40]. The approach adopted was to use different crack growth functions for different mechanisms observed in high and low ΔK levels with the consideration of threshold stress.

9.7 Aspects of Multiple Overload Interaction

de Koning introduced the multiple overload effect in CORPUS because constant-amplitude tests with overloads had shown that such an effect does occur. In flight simulation tests CORPUS predicts a gradually increasing crack opening level. However, the stationary value is hardly reached until specimen life is consumed. de Koning didn't apply the multiple overload effect to 7075-T5 material, having low ductility and high yield strength. It is reasonable that, since plastic zone sizes will be smaller and overlapping primary zones will occur less frequently, multiple overload effect will be negligible in 7075-T6 material.

X. RECOMMENDATIONS

The assumption in the CORPUS model that an underload has persistent effect on hump opening level seems to be incorrect. A function, determining relaxation process of hump opening stress is necessary.

The retardation function in CORPUS was assumed to be a block function which drastically simplifies the calculations. More appropriate functions other than delay switch may be meaningful for prediction models.

In the CORPUS model, the transition from plane strain to plane stress only affects plastic zone sizes. It does not affect the hump opening function, S_{op}. This may be regarded as a shortcoming of the model. As discussed earlier, shear lips have an effect on crack opening behaviour.

The effects of sheet thickness, crack tip blunting, ductile tearing are not covered in the model. The relevance of these effects should be investigated.

XI. CONCLUSIONS

1. The discussion on the crack propagation models has demonstrated that crack opening models are more reliable and more compatible with the crack growth mechanisms. This is also indicated by other investigators [41].

2. The performance of the CORPUS model in predicting crack growth life, in general is quite good. The ratios of predictions and test result are in the range between 0.5 and 2 for almost all data observed in the present study.

3. Introduction of multiple overload effect in the CORPUS model substantially improves the predictions for 2024-T3 material with high ductility and low yield strength.

4. Empirical trends are correctly predicted with the exception of some sequence and underload effects.

5. Some shortcoming are also indicated.

   a) The CORPUS model gives too much weight to a rarely occurring negative load if that load is more compressive than the frequently occurring ground stress level. The prediction in this case is conservative.

   (b) Some sequence effects are predicted, but not observed.

   (c) Crack extensions in high ΔK values were underpredicted.

5. The accuracy obtained in the CORPUS model seems to be quite acceptable for practical applications. It is not reasonable to require highly accurate predictions, while load spectra and other service variables are liable to errors and data scatter, as long as the models show the correct trends for variations of spectrum and test parameters.

6. The CORPUS model has proved the importance of understanding of the crack growth phenomenon for prediction models. But, more understanding is required for

the interrelations between microstructure, fracture mechanisms, plane stress/plane strain transition, threshold, crack tip blunting and crack opening behaviour.

APPENDIX

The flow Diagram of the CORPUS model

A → start

i=i+1

read σ^i_{max} and σ^i_{min}

no ← $\sigma^i_{max} < \sigma^{i-1}_{op}$ → yes

calculate crack increment $\Delta a = f(\sigma^i_{max}, \sigma^{i-1}_{op})$

$\Delta a = 0$

failure → yes → stop

no

no ← $a^i > a^j + D^j (P)$

yes

reset history value of PPZ

C

C

$\sigma^i_{max} > \sigma H^j_{max}$ (P)

yes

no

new PPZ
overrule PPZ history
values of j and
remaining ones.
Calculate plastic zone

no

$\sigma^i_{min} < \sigma H^j_{min}$

no

all history
values of PPZ
are checked

yes

B

yes

reset σH^j_{min}
reset σH^j_{op}
Overrule All SPZ
history values

-set the history values
 of the new PPZ.
-calculate hump opening
 stress of the cycle i
-update overload
 interaction factor

A

Calculate plastic
zone size, D^i

D

D

$a^i + D^i > a^j + D^j$ (P)

yes

no

new PPZ

B

Calculate secondary
plastic zone size

$a^i > a^k + D^k$ (S)

no

yes

Reset the history
values of SPZ

E

E

$\sigma^i_{max} > \sigma H^k_{max}$ (S)

yes

no

Overrule SPZ history value k and remaining ones

no

All SPZ history values are checked

no

$\sigma^i_{min} < \sigma H^k_{min}$ (S)

yes

yes

reset σH^k_{min}
reset σH^k_{min}

Calculate hump opening stress of cycle i, S^i_{op}

calculate hump opening stress of the cycle i

no

$\sigma H^k_{op} < \sigma H^j_{op}$

yes

$\sigma^i_{op} > \sigma H^j_{op}$ (P)

no

$S^i_{op} > S^j_{op}$ (P)

no

yes

Overrule SPZ history values of k

yes

new SPZ set history values

new SPZ set history values

select the highest S_{op} from PPZ and SPZ be used for calculation of crack increment in the next cycle
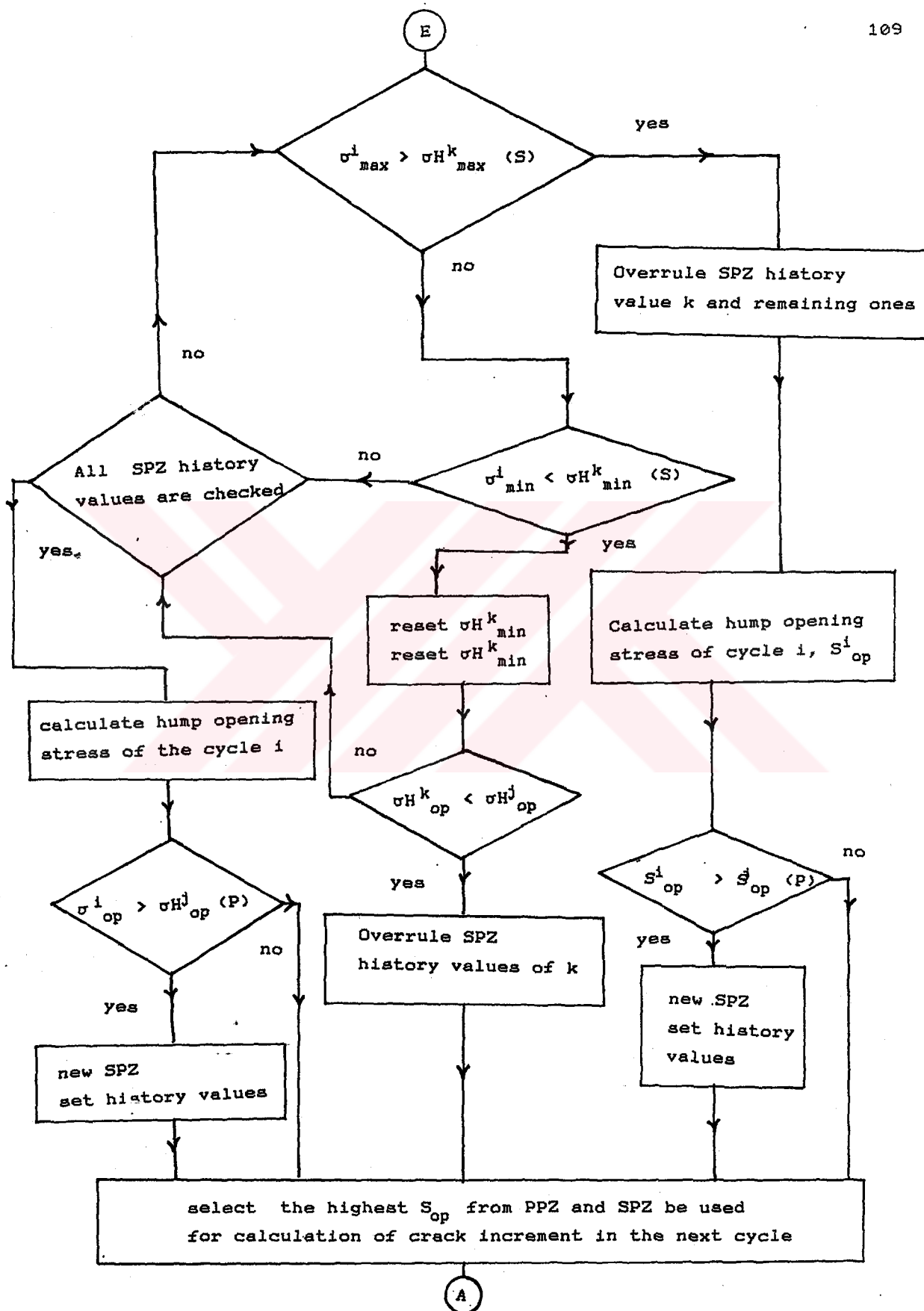
A

REFERENCES

1. J. Schijve, "Four lectures on Fatigue Crack Growth", Engineering Fracture Mechanics, Vol.11, 1979, pp.167-221.

2. J. Telesman and S.D. Antolovich, "A Study of Spectrum Fatigue Crack Propagation in Two Aluminum Alloys", Engineering Fracture Mechanics, Vol.24, No.3, 1986, pp 453-462.

3. D. Broek, "A Similitude Criterion for Fatigue Crack Growth Modelling", Fracture Mechanics: Sixteenth Symposium, ASTM STP 868, American Society for Testing and Materials, Philadelphia, 1985, pp. 347-360.

4. Y.P. Srivastava and S.B.L. Garg "Crack Propagation Law Using Crack Tip Opening Displacements", The Mechanism of Fracture, Proceedings of the Fracture Mechanism Program, at the International Program and Exposition on Fatigue, Corrosion Cracking, Fracture Mechanics and Failure Analysis, American Society for Metals, 1986, pp. 181-192.

5. P.C Paris and F. Erdogan, "A Critical Analysis of Crack Propagation Laws", Journal of Basic Engineering, Transaction ASME, Series D, Vol 85, 1963, p. 528.

6. W. Elber, "The Significance of Fatigue Crack Closure", ASTM STP 486, American Society for Testing and Materials, 1971, pp. 230-242.

7. U.H. Padmadinata, "Investigation of Crack-Closure Prediction Models for Fatigue in Aluminum Alloy Sheet under Flight-Simulation Loading", Delft University of Technology Report LR-619, 1990, the Netherlands.

8. ö. Vardar, Fracture Mechanics, Bogazici University Publication, 1988.

9. D. Broek, Elementary Engineering Fracture Mechanics, Martinus Nijhoff Publisher, Dordrecht, pp. 270-272.

10. A.U. De Koning and H.H. van der Linden, "Prediction of Fatigue Crack Growth Under Variable Amplitude Loading

Using a Simple Crack Closure Model", National Aerospace Laboratory Report, NLR MP 81023 U, 1981.

11. H.A. Wood, "A Summary of Crack Growth Prediction Techniques", <u>AGARD Lecture Series</u>, Vol. 62, 1973, pp. 8.1-8.31.

12. L.P. Pook, "Fatigue Crack Growth Data for Variou Materials Deduced from the Fatigue Lives of Precrack Plates", Proceedings of the 1981 National Symposium of <u>Fracture Mechanics</u>, Part 1, ASTM STP 513, 1972, pp. 106-124.

13. R.C. Rice and R. Stephens. "Overload Effects on critical Crack Growth in Austenitic Manganese Steel", Progress in Flow Growth and Fracture Toughness Testing, ASTM STP 536, 1973, pp. 95-114.

14. N.E. Frost, K.J. Marsh and L.P. Pook, "<u>Metal Fatigue</u>", Clarendon Press-Oxford, 1974, pp. 264-265.

15. S. Suresh, "Crack Deflection Implications for the Growth of Long and Short Fatigue Cracks", <u>Metallurgical Transactions</u>, Vol. 14 A, 1983, pp.2375-2385.

16. H.L. Ewalds and R.T. Furnee, "Crack Closure Measurements Along the Fatigue Crack Front of Centre Cracked Specimens", <u>Int. J. of Fracture</u>, Vol.14, pp. 53-55.

17. Ö. Vardar, "Effect of Single Overload in Fatigue Crack Propagation", <u>Engineering Fracture Mechanics</u>, Vol. 30, 1988, pp. 329-335.

18. D. Can, "Effect of Single Overload on Fatigue Crack Propagation in Al 7075-T6", MS. Thesis, Bogazici University, 1987.

19. N. Yildirim "Effect of Periodic Overloads on Fatigue Crack Propagation", MS. Thesis, Bogazici University, 1989.

20. V.M. Trebules, R. Roberts and R.W. Herzberg "Effect of Multiple Overloads on Fatigue Crack Propagation in 2024-T3 Aluminum Alloy", ASTM STP 536, 1973, pp. 115-146.

21. T.R Porter, "Method of Analysis and Prediction for Variable Amplitude Fatigue Crack Growth", <u>Eng. Fracture Mechanics</u>, Vol.4, 1972, pp. 717-736.

22. H. Lowak, J.B Frantz and D. Schütz, "mini-TWIST: A Shortened Version of TWIST", Laboratorium für Betriebfestigkeit, Report No. T13-146, Germany, 1979.

23. O.E. Wheeler, "Spectrum Loading and Crack Growth", <u>Journal of Basic Engineering</u>, 94D, pp.181-186.

24. T.D. Gray and J.P. Gallagher, "Predicting Fatigue Crack Retardation following a single overload using a modified Wheeler model", <u>Mechanics of Crack Growth</u>, ASTM STP 590, Philadelphia, 1976, pp. 331-344.

25. J.E. Chang, R.M Eagle and J. Stolpesad, "Fatigue Crack Growth Behaviour and Life Predictions for 2219-T851 Aluminum Subjected to Variable Amplitude Loadings", <u>Fracture Mechanics</u> : Thirteen Conference, ASTM 743, 1981, pp. 3-27.

26. W.S. Johnson, "Multi-parameter Yield Zone Model for Predicting Spectrum Crack Growth", Methods and Models for Predicting Fatigue Crack Growth under Random Loading", <u>Methods and Models for Predicting Fatigue Crack Growth under Random Loading</u>, ASTM 748, 1981, pp. 85-102.

27. J.B. Chang, M. Szamossi and K.W. Liu, "Random Spectrum Fatigue Life Predictions with or without Considering Load interactions", <u>Methods and Models for Predicting Fatigue Crack Growth under Random Loading</u>, ASTM 748, 1981, pp.115-132.

28. J.L. Rudd and R.M. Engle, "Crack Growth Behaviour of Centre-Cracked Panels under Random Spectrum Loading", <u>Methods and Models for Predicting Fatigue Crack Growth under Random Loading</u>, ASTM 748, 1981, pp. 103-114.

29. C.M. Hudson, "A Root-Mean-Square Approach for Predictin Fatigue Crack Growth under Random Loading", <u>Methods and Models for Predicting Fatigue Crack Growth under Random Loading</u>, ASTM 748, 1981, pp. 41-52.

30. A. Bignonnet, Y. Sixou, J.M. Verstavel, "Equivalent Loading Approach to Predict Fatigue Crack Growth under Random Loading", <u>Fatigue Crack Growth under Variable</u>

Amplitude Loading, Elsevier Applied Science, 1988, pp. 372-374.

31. F.G. Hamel, G. Theriault, J. Masounave, "A Simple Procedure for the Prediction of Fatigue Crack Growth Rate under Variable Amplitude Loading", International Conference and exposition on Fatigue Corrosion Cracking, Fracture and Failure Analysis, American Society for Metals, 1986, pp. 275, 281.

32. S.T. Rolle and J.M. Barsom, Fracture and Fatigue Control in Structures, Pentice Hall, New Jersey, 1977, pp. 276-289.

33. J.C. Newman"A Crack Closure Model for Predicting Fatigue Crack Growth under Aircraft Spectrum Loading, Methods and Models for Predicting Fatigue Crack Growth under Random Loading, ASTM 748, 1981, pp. 53-84.

34. W.L. Ko, "Application of Fracture Mechanics and Half-Cycle Theory to the Prediction of Fatigue Life of Aerospace Structural Components", International Journal of Fracture, Vol. 39, 1989, pp. 45-62.

35. A.U. Koning, "A Simple Crack Closure Model for prediction of Fatigue Crack Growth Rates under Variable Amplitude Overload", Fracture Mechanics: Thirteen Conference, ASTM STP 743, Philadelphia, 1981, pp. 63-85.

36. D. Aliaga, A. Davy and H. Shaff, "A Simple Crack Closure Model for Predicting Fatigue Crack Growth under Flight Simulation Loading", Mechanics of Fatigue Crack Closure, ASTM STP 982, pp. 491-504.

37. D. Aliaga, A. Davy and H. Shaff, "Damage Tolerance Evaluation of Aircraft Components under Spectrum Loading", ICAS Proceedings, Vol.2, 1984, pp. 922-931.

38. U.H. Padmadinata,"Fatigue Crack Growth Prediction Study Based on the Onera Model for Constant Amplitude and Simplified Simulation Case", Delft University of Technology, Report L-554, 1988.

39. G. Baudin, R. Labourdette and M. Robert, " Prediction of

Crack Growth under Spectrum Loadings with ONERA Model", <u>Fatigue Crack Growth under Variable Amplitude Loading</u>, Elsevier Applied Science, 1988, pp. 292-309.

40. A.U de Koning and D.J Dougherty, "Prediction of Low and High Crack Growth Rate under Constant and Variable Amplitude Loading", <u>Fatigue Crack Growth under Variable Amplitude Loading</u>, Elsevier applied Science, 1988, pp. 208-218.

41. R.J.H. Wanhill and J. Schijve, "Current Status of Flight Simulation Fatigue crack growth Concepts", <u>Fatigue Crack under Variable Amplitude Loading</u>, Elsevier applied Science, 1988, pp. 326-340.

42. U.H. Padmadinata, "Sequence Effects of High-Amplitude Loads in the Most Severe flights of miniTWIST on Fatigue Crack Growth in Al-alloy sheet material", Delft University of Technology Report, Report LR-493, 1986.

43. J. Siegl and J. Schijve, "Fractographic Observations on Fatigue Crack Growth under miniTWIST flight-simulation loading", Delft University of Technology Report, Report LR-631, 1990.